



Title	STUDIES ON STRUCTURE AND FUNCTION OF PEROXIDASE
Author(s)	小林, 一雄
Citation	大阪大学, 1984, 博士論文
Version Type	VoR
URL	https://hdl.handle.net/11094/2779
rights	
Note	

The University of Osaka Institutional Knowledge Archive : OUKA

<https://ir.library.osaka-u.ac.jp/>

The University of Osaka

STUDIES ON STRUCTURE AND FUNCTION OF PEROXIDASE

(ペルオキシダーゼの構造と機能に関する研究)

1984

KAZUO KOBAYASHI

CONTENTS

CONTENTS

GENERAL INTRODUCTION		1
CHAPTER	1.	Electron Paramagnetic Resonance of NO-Ferrous Heme-Nitrogen Base
	1-1.	Introduction 7
	1-2.	Materials and Methods 8
	1-3.	Results 9
	1-4.	Discussion 15
	1-5.	References 19
CHAPTER	2.	The NO-Probed Detection of the Heme-Linked Ionization of Myoglobin
	2-1.	Introduction 21
	2-2.	Materials and Methods 21
	2-3.	Results and Discussion 22
	2-4.	References 27
CHAPTER	3.	Electron Paramagnetic Resonance Studies of NO-Ferrous Heme-Polymer Complex
	3-1.	Introduction 28
	3-2.	Materials and Methods 29
	3-3.	Results and Discussion 29
	3-4.	References 33

CHAPTER	4.	Flash Photolysis Studies on NO-Ferric Hemoproteins	
	4-1.	Introduction	34
	4-2.	Materials and Methods	34
	4-3.	Results and Discussion	36
	4-4.	References	40
CHAPTER	5.	Kinetic Analysis of the Recombination of NO with Ferric Hemoproteins by the Flash Photolysis Method	
	5-1.	Introduction	41
	5-2.	Materials and Methods	42
	5-3.	Results	43
	5-4.	Discussion	52
	5-5.	References	56
CHAPTER	6.	Electron Paramagnetic Resonance and Optical Absorption spectra of the Pentacoordinated Ferric Hemoproteins	
	6-1.	Introduction	57
	6-2.	Materials and Methods	58
	6-3.	Results	60
	6-4.	Discussion	66
	6-5.	References	69
CHAPTER	7.	One Electron Reduction in Oxyform of Hemoproteins	
	7-1.	Introduction	70

7-2.	Materials and Methods	71
7-3.	Results	73
7-4.	Discussion	80
7-5.	References	84
CONCLUSION		87
LIST OF PUBLICATION		90
ACNOWLEDGEMENT		93

GENERAL INTRODUCTION

From the standpoint of chemical process engineering, enzymes have many characteristic properties which make them ideal catalysts. They can operate under extremely mild conditions of pH and temperature, can generally induce fast reaction rates, and are extremely specific in the types of reaction in which they are involved. Enzymes are able to catalyze many reactions, which do not proceed with ordinary chemical catalysts. Their unique capabilities for the catalysis of extremely specific chemical reactions have aroused the interest and challenged the ingenuity of chemist, medical scientists and industrial processors. During the past ten years scientists have a substantial increase in knowledge of enzymes and have developed new and improved methods for the purification and handling of enzymes. Such advances have opened new possibilities of application of reactions catalyzed by enzymes. For example, the enzymes bound to or entrapped within synthetic materials, immobilized enzymes, are utilized as catalysis for industrial production [1-3], for chemical analysis [4] and for clinical test [5]. As our knowledge of structure and function of enzymes has increased, the idea of preparing improved catalysis for in vitro use by modification of known enzymes has received growing support [6]. In addition, in the fields of organic and inorganic chemistry, attempts have been made to design the synthesise compounds which are structurally and functionally similar to the active site of enzymes [7-10]. In this manner studies of structure and function

of enzymes are expected to provide insight into intrinsic nature of catalysis, which may suggest new approaches to industrial chemistry.

Among enzyme molecules, enzymes containing metal ion are of interest in connection with organometallic chemistry. These metal components alone already possess primitive enzymatic activity, which is greatly enhanced by a protein. The typical examples are hemoproteins. Though hemoproteins have a common prosthetic group at the active center, each hemoprotein exhibits a variety of biological function. They participate in electron transfer [11], oxygen transport [12], and activations of oxygen [13] and hydrogen peroxide [14]. One of the fascinating problems is to clarify how subtle changes in going from one molecule to closely related one lead to such dramatic changes in behavior. One step in solving such a problem is to decipher the structure, function and behavior of each type molecule in detail on the molecular level.

This thesis deals with structure and function of peroxidase. Peroxidases are widely distributed in plants, animals, molds bacteria and microorganisms, and catalyze oxidation of various molecules by hydrogen peroxide as its specific oxidizer. These enzymes play important role in the metabolism of defence substrate [15, 16] and hormone [17-19], and biosynthesis of lignin [20]. Among peroxidases, horseradish peroxidase (HRP) is of great interest in the following aspects.

- (1) The reaction catalyzed by HRP is the first example proposed to proceed by free radical mechanism among biological reactions [21].
- (2) HRP has five oxidation-reduction states. Among them, two states formed in enzymatic cycle have received much attentions, because of their unusual ferryl state (Fe^{4+}).
- (3) Although HRP contains the iron protoporphyrin with a coordinated histidine as an axial ligand of the heme iron in the same way as myoglobin (Mb), ferrous HRP binds molecular oxygen irreversibly but Mb bind it reversibly. HRP is biologically active in the ferric state, whereas Mb are active in the ferrous state.

In the present work, a structural origin for the great differences in biological functions between HRP and Mb has been elucidated by the use of EPR spectra, flash photolysis and pulse radiolysis methods.

CHAPTERS 1, 2 and 3 deal with the electronic structure of NO-ferrous hemoproteins and their model compounds studied by the use of EPR spectra. In CHAPTER 1, EPR spectra of NO-ferrous heme nitrogen base as model compounds of hemoproteins are described, which interpret the EPR spectra of NO-ferrous HRP. CHAPTER 2 deals with EPR spectra of NO-ferrous Mb, where pH-dependence of EPR spectra is described. In CHAPTER 3, application of EPR measurements on the NO-ferrous heme to the synthetic polymer systems is described, where an attempt is made

to correlate the alteration of NO-heme linkage and the conformational change of the polymer chain.

CHAPTERS 4, 5 and 6 deal with photolysis of NO-ferric hemoproteins. In CHAPTER 4, photodissociability of the various complexes of ferric hemoproteins as observed in the ferrous state is described. CHAPTER 5 describes the kinetic experiments on the flash photolysis of NO-ferric hemoproteins at room temperature, of which results are compared with those obtained by stopped flow experiments. In CHAPTER 6, photolysis of NO-ferric hemoproteins at liquid helium temperature is described, where optical and EPR characteristics of the pentacoordinated heme are given.

CHAPTER 7 deals with the higher oxidation states of hemoproteins studied by the use of pulse radiolysis method. Reaction of the hydrated electron with oxyform of hemoproteins is described.

References

- [1] I. Chibata et al., "Koteikakoso", Kodansha, 1975.
- [2] T. Fukumura, Agric. Biol. Chem., 40, 1687 (1976).
- [3] H. Suzuki, Y. Ozawa, H. Oota, and H. Yoshida, Agric. Biol. Chem., 33, 506 (1969).
- [4] I. Karube, S. Matsuda, T. Matsunaga, and S. Suzuki, J. Ferment. Technol., 55, 243 (1977).
- [5] T. Uwazima and O. Terada, Agric. Biol. Chem., 39, 1511 (1975).
- [6] H. Holzer and W. Duntze, Ann. Rev. Biochem., 40, 345 (1971).
- [7] J. H. Wang, Accounts Chem. Res., 3, 90 (1970).

- [8] D. E. Metzler, J. B. Longenecker, and E. E. Snell, *J. Am. Chem. Soc.*, 76, 2016 (1954).
- [9] R. R. Grinstead, *Biochemistry*, 3, 1308 (1964).
- [10] J. P. Collman, R. R. Gagne, C. A. Reed, T. R. Halbert, G. Lang, and W. T. Robinson, *J. Am. Chem. Soc.*, 97, 1427 (1975).
- [11] B. Hagihara, N. Sato, and J. Yamanaka, "The Enzymes", P. D. Boyer, eds., Vol. XI, p. 549, Academic Press, New York, 1975.
- [12] A. Antonini and M. Brunori, "Hemoglobin and Myoglobin in Their Reactions with Ligands", North-Holland Publ. Co., Amsterdam and London, 1971.
- [13] O. Hayaishi, M. Nozaki, and M. T. Abbott, "The Enzymes", P. D. Boyer, eds., Vol. XII, Part B, p. 119, Academic Press, New York, 1975.
- [14] M. Morrison and G. R. Schonbaum, *Ann. Rev. Biochem.*, 45, 861 (1976).
- [15] C. B. Hamon and S. J. Klebanoff, *J. Exp. Med.*, 137, 438 (1973).
- [16] T. Oghuchi and T. Asada, *Physiol. Plant Pathol.*, 5, 183 (1975).
- [17] A. Taurog, "Recent Progress in Hormone Research", E. B. Astwood, eds., Vol. XXVI, p. 189, Academic Press, New York, 1970.
- [18] J. P. Gove and M. C. Hoyle, *Plant Physiol.*, 56, 684 (1975).
- [19] J. Sequeira, *Ann. Rev. Plant Physiol.*, 24, 353 (1973).
- [20] C. P. Vance and R. J. Scherwood, *Plant Physiol.*, 58, 915 (1976).
- [21] I. Yamazaki, "Free Radicals in Biology", W. A. Pryor eds.,

Vol. III, p. 183, Academic Press, 1977.

CHAPTER 1. Electron Paramagnetic Resonance of NO-Ferrous Heme-Nitrogen Base

1-1. Introduction

Hemoproteins such as Mb, cytochrome and HRP have a common prosthetic group, protoheme, at the active center. The variety of biological function acquired by these proteins arises from the nature of the axial ligand and the structure of the heme pocket. The NO complexes of the ferrous hemoproteins in Fig. 1-1 serve as paramagnetic probes which can provide considerable insight into the nature of the trans axial ligand and the interaction of the ligated NO with surrounding amino acid residues. For example, the EPR absorption has been used to study the stereochemistry of the 6th ligand [1-3]. Those were single crystal measurements, while random oriented frozen solutions of NO-ferrous hemoproteins have been studied extensively by many investigators. For example, the conformational change by denaturation and that due to allosteric effectors have also been studied by this technique [4-9]. On the other hand, the peculiar heme-enzymes [10-14] have been studied by the EPR absorption on the NO complex.

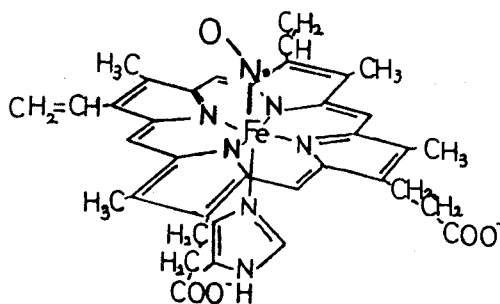


Fig. 1-1. Representation of the NO-ferrous heme-imidazole complex.

In this chapter, in order to interpret the EPR spectra of NO-ferrous HRP and the related systems, the EPR spectra of NO-ferrous heme-nitrogen base as model compounds of hemoproteins were measured using second derivative display. An effort was made to detect the effects of proximal basicity, steric hindrance of the proximal base, and side chain electron donation by EPR method.

1-2. Materials and Methods

Protohemin was purchased from Sigma and used without further purification. Other modified porphyrins were prepared according to the method of Caughey et al. [15]. These deuterohemin derivatives were purified by chromatography on a silica gel column.

The small amount of freshly prepared hemin solution was mixed with solvent containing various bases. Final concentrations of hemin and base were 10^{-5} and 10^{-2} M, respectively. After degassing by using a conventional vacuum line, reduction of hemin was performed by addition of a small amount of sodium dithionite and then NO gas was introduced to yield the NO-ferrous heme, according to the method of Kon et al. [16].

A Varian E-line spectrometer was used for the EPR measurements, where, in the second derivative, 1 KHz field modulations were employed, together with the 100 KHz field modulation for first derivative display. Microwave power was set to 5 mW. All the measurements were made at liquid nitrogen temperature.

1-3. Results

1-3-1. The effect of proximal basicity on EPR spectra of NO-ferrous heme-nitrogen base

Fig. 1-2 shows the EPR spectra of NO-ferrous protoheme complexes with 4-cyanopyridine (1) and 4-aminopyridine (2) in N,N'-dimethylformamide (DMF) displayed by first and second derivatives. The second derivative spectra show well resolved 9 lined hyperfine structure (hfs) around g_z , which can be interpreted as the coupling of the nitrogen atom ($I = 1$) of NO and the pyridine derivatives of the 5th coordinated ligand. Its hfs in Fig. 1-2-(2) is seen more distinctly than that of Fig. 1-2-(1). In addition, g_x and g_y values are found to be also affected by 4-substitution of pyridine derivatives, as shown in Fig. 1-2. In this figure, both g_x and g_y values of NO-ferrous protoheme-4-aminopyridine are smaller than those of NO-ferrous protoheme-4-cyanopyridine.

Fig. 1-3 shows the region of the magnetic field at g_z on an expanded scale, where the hfs was observed in Fig. 1-2. From these hfs, the coupling constants of nitrogen atom in the 6th ligand (A_{N_1}) and the 5th ligand (A_{N_2}) were determined. Similarly, imidazole derivatives were also used as the 5th coordinated base. These coupling constants are summarized in Table 1-(1). It is noted that A_{N_1} and A_{N_2} and g values change significantly among NO-ferrous protoheme-4-substituted pyridine and imidazole derivatives. These EPR parameters are plotted against the pK_a values of these pyridine derivatives in Fig. 1-4. Both A_{N_1} and A_{N_2} increase and g_x and g_y values decrease as

the basicity of nitrogen atom (pK_a values) of the 5th coordinated base increases.

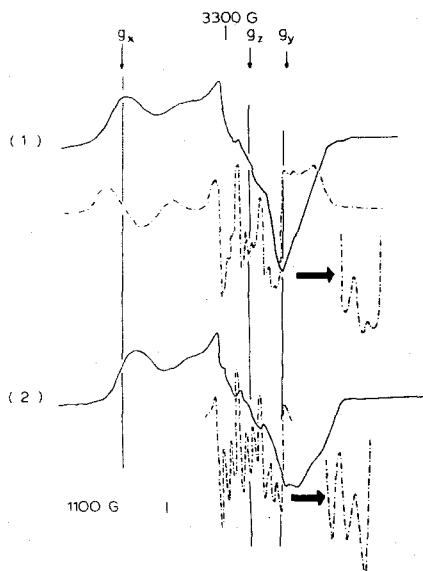


Fig. 1-2. The EPR spectra of NO-ferrous protoheme-pyridine derivatives. (1) 4-cyanopyridine; (2) 4-aminopyridine.

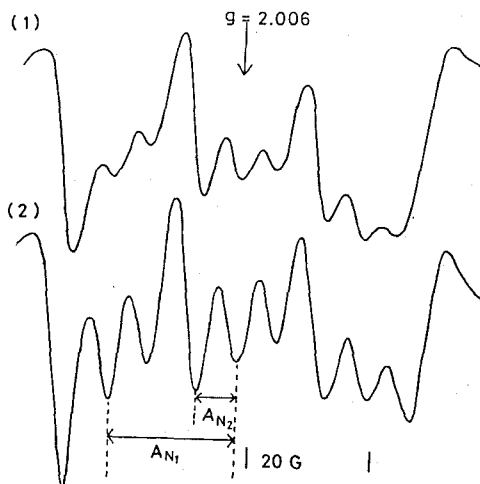


Fig. 1-3. Second derivative EPR spectra of NO-ferrous protoheme-pyridine derivatives. (1) 4-cyanopyridine; (2) 4-aminopyridine.

Table 1-(1)

The pK_a values for the basicity of nitrogen atom of the 5th coordinated base and the EPR parameters of NO-ferrous protoheme-pyridine and imidazole derivatives

4-substituent pyridine	Principal g value			Coupling constant (G)		pK_a
	g_x	g_z	g_y	A_{N_1}	A_{N_2}	
-NH ₂	2.076	2.006	1.976	21.9	6.7	9.12
-CH ₃	2.078	2.006	1.983	21.7	6.5	6.03
-H	2.078	2.006	1.984	21.7	6.5	5.21
-COCH ₃	2.079	2.006	1.987	21.5	6.2	3.51
-CN	2.083	2.006	1.989	21.3	6.0	1.96

1-substituent imidazole						
-CH ₃	2.074	2.006	1.976	21.9	7.0	7.33
-H	2.074	2.006	1.976	21.9	6.9	6.95
-COCH ₃	2.077	2.006	1.977	21.5	6.8	3.6

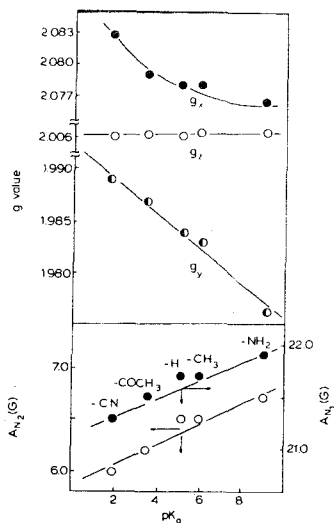


Fig. 1-4. The correlation between the EPR parameters and the pK_a values of pyridine derivatives.

1-3-2. The electron withdrawing effect on the heme ring in EPR spectra of NO-ferrous heme-imidazole

2,4-substitution of the heme-ring also influenced EPR spectrum, indicating that the nucleophyllicity of the porphyrin side chain has appreciable effect on metal-ligand bond strength. A_{N_1} and A_{N_2} increase and g_x and g_y values decrease with changes in the 2,4-substituent in the order ethyl < hydrogen < vinyl < acetyl (Table 1-(2)). This order is found to represent the order of increasing electron withdrawing effect of the 2,4-substituents. These EPR parameters are plotted against pK_3 , that is a measure of relative basicities for metal-free porphyrin, as shown in Fig. 1-5.

Table 1-(2)

The pK_3 values for metal-free derivatives of substituted deuteroporphyrin and EPR parameters of NO-ferrous substituted deuteroheme-imidazole

2,4-substituent deuteroheme	Principal g value			Coupling constant (G)		pK_3
	g_x	g_z	g_y	A_{N_1}	A_{N_2}	
-CH ₂ CH ₃	2.076	2.006	1.977	21.5	6.6	5.8
-H	2.075	2.006	1.977	21.5	6.7	5.5
-CH=CH ₂	2.074	2.006	1.976	21.9	6.9	4.8
-COCH ₃	2.073	2.006	1.976	22.1	7.0	3.3

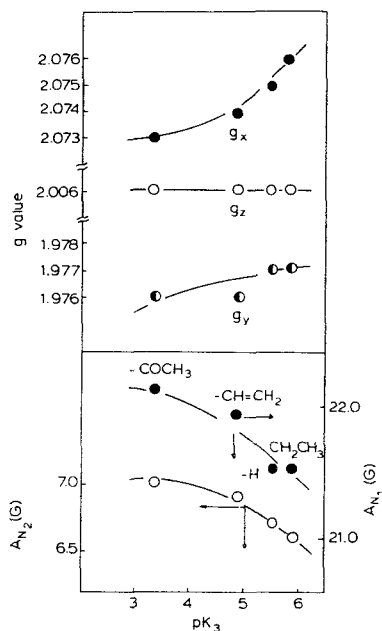


Fig. 1-5. The correlation between the EPR parameters and the pK_3 values for metal free derivatives of 2,4-substituted deuterohemes.

1-3-3. The effect of steric hindrance on EPR spectra of NO-ferrous heme-nitrogen base

Fig. 1-6 shows the EPR spectra of NO-ferrous protoheme-1-methylimidazole (1) and 2-methylimidazole (2) in DMF. The hfs of the second derivative spectrum in Fig. 1-6-(1) is seen more distinctly than that of Fig. 1-6-(2). This difference between these EPR spectra is considered to be due to the steric hindrance of 2-methylimidazole. Table 1-(3) compares A_{N_1} , A_{N_2} and g values of these EPR spectra. The decrease of A_{N_2} from 7.0 G to 6.4 G and the increase of A_{N_1} from 21.9 G to 22.5 G are seen when the 5th ligand was changed from 1-methylimidazole to 2-methylimidazole. The g_x and g_y also increase.

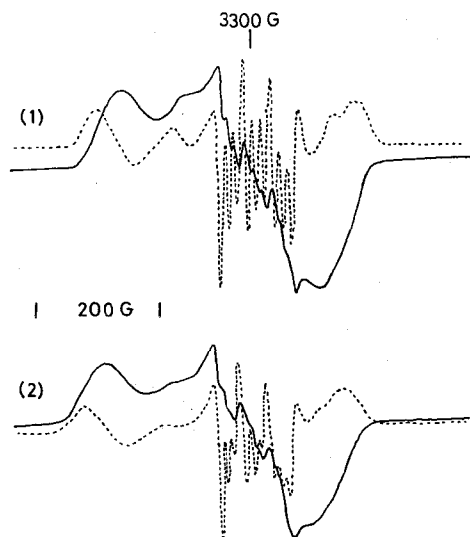


Fig. 1-6. The EPR spectra of NO-ferrous protoheme-imidazole derivatives. (1) 1-methylimidazole; (2) 2-methylimidazole.

Table 1-(3)

The effect of steric hindrance of the proximal ligand on EPR parameters

	Principal g value			Coupling constant (G)	
	g_x	g_z	g_y	A_{N_1}	A_{N_2}
1-methylimidazole	2.074	2.006	1.976	21.9	7.0
2-methylimidazole	2.078	2.006	1.978	22.5	6.4

When imidazole derivatives having more bulky groups at the 2 position such as 2-phenylimidazole were added to NO-ferrous heme with a [2-phenylimidazole]/[NO-ferrous heme] molar ratio of 500, the EPR spectra, which exhibited three hyperfine splitting, are essentially identical to that of the pentacoordinated heme (NO-ferrous heme). This suggests that 2-phenylimidazole does not coordinate. On the other hand, when 2-substituted pyridine

derivatives such as 2-methylpyridine and 2-ethylpyridine were used, the steric effect on EPR spectra of NO-ferrous heme-pyridine derivatives could not be discerned.

1-4. Discussion

The high resolution of the second derivative display is well demonstrated in this chapter. Though the high resolution of the second derivative display in EPR spectroscopy has well been recognized, this method has been applied to biochemical systems infrequently. This may come from mainly the poor sensitivity arising from the low frequency (80 Hz) and fixed second modulation amplitude employed previously, thus the small changes in the EPR spectra of NO-ferrous heme-base caused by the basicity of the base could not be detected [17]. Recently, Chevion et al. suggested the usefulness of the second derivative display using third harmonic detection in EPR studies. In the present experiments, the poor sensitivity of the second derivative is almost overcome by the use of high frequency second modulation (1 KHz). The high resolution can be obtained by setting the second modulation amplitude to approximately twice that of the first modulation amplitude. Here, (first modulation, 2 G and second modulation, 5 G), the sensitivity is almost comparable to the ordinal first derivative display.

In this chapter, it is demonstrated that EPR spectra vary with changes of the nature of the bond between a NO-ferrous heme and a coordinated nitrogen base. The EPR parameters determined by the present method are compared with the bond length in.

Fe-N_b obtained by X ray diffraction [19-20]. The Fe-N_b bond length in NO-ferrous heme-1-methylimidazole and NO-ferrous heme-4-methylpiperidine are 2.328 \AA and 2.463 \AA , respectively. The increment of this bond length reflects the decrease of the coupling constants from ($A_{N_1} = 21.9 \text{ G}$, $A_{N_2} = 7.0 \text{ G}$) to ($A_{N_1} = 21.3 \text{ G}$, $A_{N_2} = 6.3 \text{ G}$) and on the increase of g values from ($g_x = 2.074$, $g_y = 1.976$) to ($g_x = 2.078$, $g_y = 1.980$). This suggests that the longer bond length for Fe-N_b bond results in the increase of g values and the decrease of A_{N_1} and A_{N_2} . 2-Methylimidazole may also cause a elongation of Fe-N_b bond relative to the sterically undemanding 1-methylimidazole, because of the steric interaction of the 5th ligand. The mode of this effect, however, is different from that of basicity changes; A_{N_1} increases concomitant with the decrease of A_{N_2} as an effect of the steric hindrance, while both A_{N_1} and A_{N_2} decrease as an effect of basicity changes. Furthermore, the change in the coupling constants from 1-methylimidazole to 2-methylimidazole is larger than the change from 1-methylimidazole to 1-acethylimidazole (Tables 1-(1) and (3)). The difference between these effects may be due to the geometrically distortion of the iron-histidine binding. The electron withdrawing group such as acetyl group in N position of the imidazole decreased the strength of the σ bond at the 5th coordinated site. On the other hand, the steric hindrance of the 2-methylimidazole led to a decrease of the $p_\pi-d_\pi$ interaction of the iron with the 5th ligand.

NO-ferrous hemoproteins such as Mb, cytochrome c (cyt c) and

HRP, which are known to be consist of NO-ferrous heme-imidazole, exhibit characteristic EPR spectra. Among these EPR spectra, it is noted that EPR spectrum of NO-ferrous cyt c could be reproduced in the present model systems (NO-ferrous heme-imidazole in DMF). This finding demonstrates that NO-ferrous heme-base complexes are indeed adequate model systems of NO-ferrous hemoproteins, so far as the electronic structure of heme part is considered. The differences in the EPR spectra of NO-ferrous hemoproteins are considered to result from two possible factors. These factors are as follows; (1) the nature of the iron-proximal histidine binding, (2) the interaction of the ligated NO with surrounding amino acid residues. From the values of coupling constants, the iron-proximal histidine distance in these NO-ferrous hemoproteins may increase in the order: Mb ($A_{N_1} = 18.9$ G, $A_{N_2} = 6.6$ G) > cyt c ($A_{N_1} = 21.9$ G, $A_{N_2} = 6.8$ G) > HRP ($A_{N_1} = 22.0$ G, $A_{N_2} = 7.0$ G). Recently similar proposal has been offered for the Fe-N_ε (proximal histidine) stretching vibration of ferrous Mb and ferrous HRP [21]. It is unlikely, however, that the characteristic EPR spectrum of NO-ferrous HRP originates from the iron-proximal ligand only, because the anisotropy of g values in NO-ferrous HRP cannot be interpreted solely by the effects of the proximal basicity, steric hindrance of the proximal base and side chain electron donation. In model systems, the parallel relationships between g values and coupling constants are seen; both g_x and g_y decreased concomitant with the increase of A_{N_2} . In the case of NO-ferrous HRP, the coupling constants are larger

than those of other hemoproteins and three principal g values are well separated; the high field signal shifts to the right ($g_y = 1.958$) and the low field signal shifts to the left ($g_x = 1.980$). This suggests that substantially the changes in EPR spectrum of NO-ferrous HRP may be attributed to the interaction of the NO ligand with surrounding amino acid residues, not to the nature of the iron-proximal histidine binding. The interaction between the protein residue and the NO ligand may contribute to the particular stereochemistry of the Fe-N-O bond, which determines the anisotropy of g values. The Fe-N-O bond angle of ferrous hemoproteins are different from those of model systems. For example, in the X ray study of NO-ferrous tetraphenylporphyrin-1-methylimidazole [22], the Fe-N-O bond angle is 140° . From the EPR spectra of the single crystal of NO-ferrous Mb, it has been known that the presence of the distal base can force the ligand away from its preferred position perpendicular to the heme plane. In the case of HRP, the importance of the interaction between the distal base and heme-ligand has been indicated by Yamazaki et al. [23, 24]. Furthermore, this is also supported by EPR spectrum of NO-ferrous HRP at room temperature. Even at room temperature the spectrum has a larger anisotropy as compared with those of Mb and the model compounds, suggesting that the rotation of NO molecule in NO-ferrous HRP is strongly restricted by surrounding amino acid residues. It appears that Fe-N-O unit is more bent than those of other hemoproteins. A computer analysis to evaluate exact g and A values of EPR spectrum in NO-ferrous HRP provides a clue.

1-5. References

- [1] J. C. W. Chien, *J. Chem. Phys.*, 51, 4220 (1969).
- [2] L. C. Dickinson and J. C. W. Chien, *J. Am. Chem. Soc.*, 93, 5036 (1971).
- [3] J. C. W. Chien and L. C. Dickinson, *J. Biol. Chem.*, 252, 1331 (1977).
- [4] T. Shiga, K. J. Hwang, and I. Tyuma, *Biochemistry*, 8, 378 (1966).
- [5] H. Rein, O. Ristan, and W. Scheler, *FEBS Lett.*, 24, 24 (1972).
- [6] E. Trittelvity, H. Sick, and K. Gersonde, *Eur. J. Biochem.*, 31, 578 (1972).
- [7] T. Taketa, W. E. Antholine, A. G. Mauk, J. A. Linbnoch, *Biochemistry*, 14, 3229 (1975).
- [8] K. Nagai, H. Hori, S. Yoshida, H. Sakamoto, and H. Morimoto, *Biochim. Biophys. Acta*, 532, 17 (1978).
- [9] K. Nagai, H. Hori, H. Morimoto, K. Hayashi, and F. Taketa, *Biochemistry*, 18, 1304 (1979).
- [10] T. Yonetani, H. Yamamoto, J. E. Erman, J. S. Leigh, and G. H. Reed, *J. Biol. Chem.*, 247, 2447 (1972).
- [11] R. Chiang, R. Makino, W. E. Spmer, and L. P. Hager, *Biochemistry*, 14, 4166 (1975).
- [12] D. O. O'Keeffe, R. E. Ebel, and J. A. Peterson, *J. Biol. Chem.*, 253, 3509 (1978).
- [13] Y. Henry and G. Mazza, *Biochim. Biophys. Acta*, 371, 14, (1974).

- [14] Y. Henry, Y. Ishimura, and J. Peisach, *J. Biol. Chem.*, 251, 1578 (1976).
- [15] W. S. Caughey, J. O. Alben, W. Y. Fujimoto, and J. L. York, *J. Org. Chem.*, 31, 2631 (1966).
- [16] H. Kon and N. Kataoka, *Biochemistry*, 14, 4166 (1969).
- [17] T. Yoshimura, T. Ozaki, Y. Shintani, and H. Watanabe, *Arch. Biochem. Biophys.*, 193, 301 (1979).
- [18] M. Chevion, M. M. Traum, E. Blumberg, and J. Peisach, *Biochim. Biophys. Acta*, 490, 272 (1977).
- [19] W. R. Scheidt and P. Piciulo, *J. Am. Chem. Soc.*, 98, 1913 (1976).
- [20] W. R. Scheidt, A. C. Brinegar, E. B. Ferro, and J. F. Kirner, *J. Am. Chem. Soc.*, 99, 7315 (1977).
- [21] J. Teraoka and T. Kitagawa, *J. Biol. Chem.*, 256, 3969 (1981).
- [22] H. Yamada and I. Yamazaki, *Arch. Biochem. Biophys.*, 165, 728 (1974).
- [23] H. Yamada and I. Yamazaki, *Arch. Biochem. Biophys.*, 171, 737, (1975).

CHAPTER 2. The NO-Probed Detection of the Heme-Linked Ionization of Myoglobin

2-1. Introduction

The heme-linked ionization group has been characterized mostly by the pH dependence of the affinity towards various ligands, together with the direct proton titration and oxidation-reduction potential [1-4]. With Mb, the absence of Bohr effect suggests that the lack of the tightly coupled heme-linked ionization group with ligation in the ferrous states, in contrast to the ferric state, where the pH-dependent changes of the dissociation constants have been well analyzed with various ligands [1, 2].

In this chapter, the detection of the heme linked ionization group is attempted with NO-ferrous Mb complex, where the pH-dependence of the hfs of the EPR spectra was examined in detail over the wide pH-range.

2-2. Materials and Methods

Sperm whale oxymyoglobin (MbO_2) was prepared from the meat by the method of Yamazaki et al. [5]. Fresh sperm whale meat was homogenized with 2 liters of cold water per kg of the muscle. As the pH of the homogenate of fresh sperm whale meat is usually below 6.0, 2 N ammonium hydroxide was added to keep the pH of the homogenate at pH 7.5. The homogenate was squeezed through a thick cloth in a press, and the extract was 70 % saturated with ammonium sulfate by addition of the solid salt; the pH was adjusted to 7.5

with ammonium hydroxide. The resulting precipitate, which contained mostly hemoglobin, was centrifuged down and discarded (4000 r.p.m. for 15 minutes). The supernatant was then saturated with ammonium sulfate, and the pH was adjusted to 7.5. The mixture was stirred with Celite for 1/2 hour and the precipitate collected by vacuum filtration. The precipitate obtained was dissolved in a small volume of cold distilled water, and the solution was dialyzed with several batches of distilled water and then with 0.005 M Tris-HCl buffer, pH 8.4, in the cold. At this stage more than 90 % of Mb was in the reduced form and stable against autoxidation. The dialyzed solution was applied to a column of DEAE-cellulose which had been equilibrated with 0.005 M Tris buffer, pH 8.4. Approximately 50 % of total Mb was slow moving and was eluted by 0.005 M Tris buffer, while the other 50 % of Mb remained close to the top of the column under these conditions. This fraction was eluted by 0.05 M Tris buffer. MbO₂ thus prepared was crystallized from 0.87 saturated solution of ammonium sulfate. All other reagents were of analytical grade.

Ferrous NO-complex of Mb was obtained by use of nitrite and sodium dithionite according to Yonetani et al. [6] or NO gas treatment [7].

EPR spectra were measured in the same manner as described in CHAPTER 1. The pH values at 77 K were employed as those at room temperature [8].

2-3. Results and Discussion

Fig. 2-1 shows the EPR spectra of NO-ferrous Mb at pH 7.5 and 10 with both first and second derivative display. Though the hfs is hardly observed with the first derivative spectrum, 9 lines of the hfs centered at g_z is clearly seen in the second derivative display. At pH 7.5, such hfs is rather unclear compared with that of pH 10.

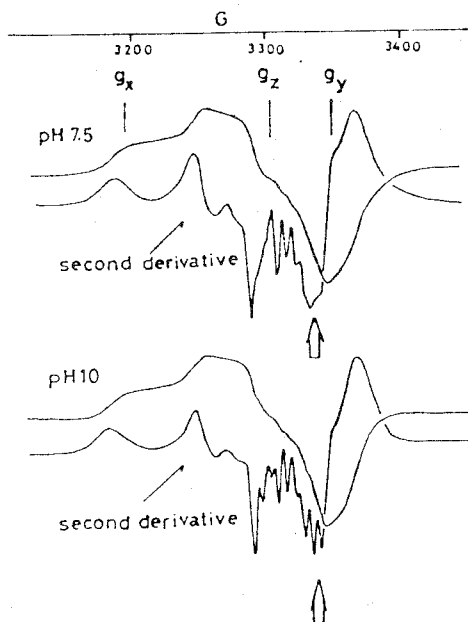


Fig. 2-1. EPR spectra of NO-ferrous Mb at pH 7.5 and 10. Phosphate buffer (pH 7.5), 0.2 M. Tris-HCl buffer (pH 10), 0.2 M.

The 9 lined hfs can be easily attributed to the coupling of nitrogen atom (nuclear spin, $I = 1$) of the imidazole group of proximal histidine and NO molecule through the heme-iron [6,7].

The pH-dependent changes of the spectra of NO-ferrous Mb are shown in Fig. 2-2, where the region of high magnetic field in Fig. 2-1 (arrowed in the figure) was recorded with the expanded scale. With increasing the pH, the peaks become more distinct than those of acidic pH.

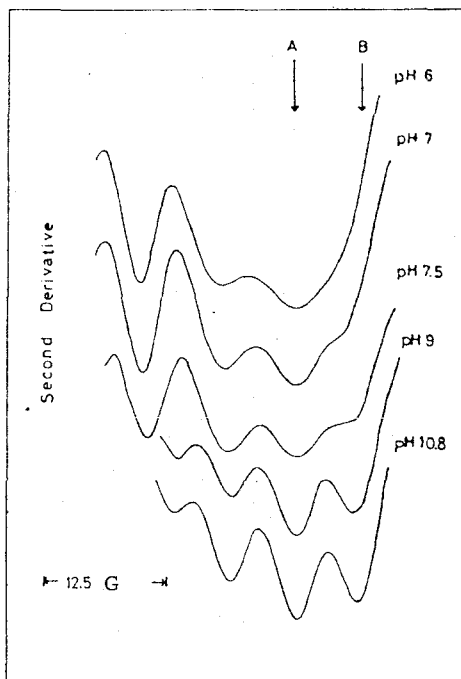


Fig. 2-2. pH dependence of the second derivative spectra of NO-ferrous Mb. The region arrowed in Fig. 2-1 was recorded in the expanded scale.

The relative EPR signal amplitude is plotted in Fig. 2-3 with the function of pH, where the data are taken from Fig. 2-2. The pK value of this transition is found to be approximately 7. In the region lower than pH 6 and above 11, the reproducible results were not obtained because of the denaturation of Mb.

The high resolution of the second derivative display is demonstrated in this chapter. Here, it is noted that the

peaks in the second derivative display correspond to the slopes of the first derivative spectra, which cannot be related directly to the spin-density. However, the above does not conflict with the following discussion, since the pH-dependent relative changes of the peak are only taken account (cf. Fig. 2-2). (cf. Fig. 2-2)

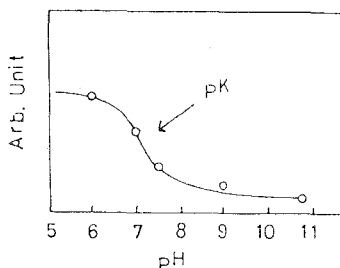


Fig. 2-3. The pH-titration of the hfs of ferrous NO-Mb. The ratio of the absorption at A and B in Fig. 2-2 is plotted against pH.

As is seen in Figs. 2-1 and 2-2, the pH-dependent changes of hfs give the direct evidence of the presence of heme-linked ionization group, which affects the electronic structure of heme-iron and NO bond. In the ferrous ligated state, the possibility has been proposed time to time that the hydrogen bond might be presented between nitrogen atom of imidazole ring of distal histidine and ligated molecule [9-12], as shown in Fig. 2-4. The value of pK obtained from the present study may support the above possibility. The other possibility of the proximal histidine seems to be unlikely, since the pK value of this proton dissociation is much more alkaline pH (≈ 12).

The presence of Bohr effect, however, may conflict with the present results, if affinity of NO is also pH-dependent, since pH-invariance of the affinity corresponds to the absence of the

interaction, at present, is that the alteration of the electronic state of heme-iron perturbed by this proton dissociation is very small as compared with the overall ligation. Those results emphasized the characteristic behavior of NO-ferrous Mb related to the presence of distal histidine (Fig. 2-4).

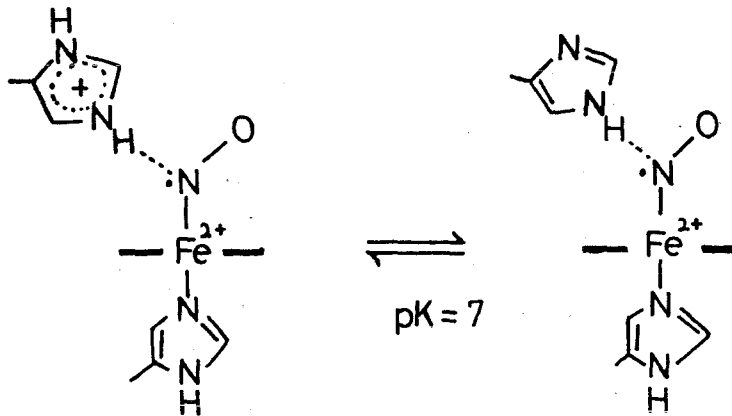


Fig. 2-4. The possible scheme for the heme-linked ionization of NO-ferrous Mb.

At acidic pH, the distal histidine becomes protonated intensifying the hydrogen bond or pushing proton to NO molecule, which may rather localize the unpaired electron on NO molecule. And, at alkaline pH, the hydrogen bond is still present but rather weak and thus the electron is delocalized into the nitrogen atom of the proximal histidine.

2-4. References

- [1] P. George and G. Hanania, *Biochem. J.*, 55, 236 (1953).
- [2] P. George and G. Hanania, *Discuss. Faraday. Soc.*, 20, 216 (1955).
- [3] H. A. Harbury, *J. Biol. Chem.*, 255, 1009 (1957).
- [4] H. Theorell and A. Ehrenberg, *Acta Chem. Scad.*, 5, 823 (1951).
- [5] I. Yamazaki, K. Yokota, and K. Shikama, *J. Biol. Chem.*, 239, 4151 (1964).
- [6] T. Yonetani, H. Yamamoto, J. E. Erman, J. S. Leigh, and G. H. Reed, *J. Biol. Chem.*, 247, 2447 (1972).
- [7] H. Kon, *J. Biol. Chem.*, 243, 4350 (1968).
- [8] Y. Orii and T. Iizuka, *J. Biochem. (Tokyo)*, 77, 1123 (1975).
- [9] J. C. W. Chien, *J. Chem. Phys.*, 51, 4220 (1969).
- [10] L. Stryer, J. C. Kendrew, and H. C. Watson, *J. Mol. Biol.*, 8, 96 (1964).
- [11] P. Nicholls, *J. Gen. Physiol.*, 49, 131 (1965).
- [12] T. Yonetani, H. Yamamoto, and T. Iizuka, *J. Biol. Chem.*, 249, 2168 (1974).

CHAPTER 3. Electron Paramagnetic Resonance Studies of NO-Ferrous Heme-polymer Complex

3-1. Introduction

The technique of the EPR measurements on the NO-ferrous heme complexes has proved its usefulness for elucidating the structure-function relationship of various hemoproteins [1-3] and model systems [4, 5]. In CHAPTERS 1 and 2, it has been shown that the second derivative display using high frequency modulation is useful method, which was applied to the NO complexes of ferrous Mb [6] and model compounds [7].

In synthetic polymer systems, the reactivity of heme-iron towards various ligands have been accepted much interest and subjected to the extensive works [8, 9]. In these works, it has been believed that the electronic structure of heme iron is altered by the conformational change of the polymer chain. However, structural information at microscopic viewpoint has not been elucidated directly.

In this chapter, the NO-ferrous heme-poly(4-vinylpyridine) (PVP) complex has been examined by EPR measurement under various conditions together with the comparison of the monomeric system in CHAPTER 1. An attempt is made to correlate the alteration of NO-ferrous heme linkage and the conformational change of the polymer chain.

3-2. Materials and Methods

4-Vinylpyridine was polymerized by the use of azobisisobutyronitrile as an initiator in methanol (MeOH). A small amount of hemin was dissolved in DMF and added to the solution containing PVP. The final concentrations of hemin and pyridine were varied between $10^{-5} \approx 10^{-4}$ M and $1 \times 10^{-2} \approx 5 \times 10^{-1}$ M, respectively. NO-ferrous heme complexes were prepared in the same manner as described in CHAPTER 1 [7].

A Varian E-line spectrometer was used for the EPR absorption measurements in the same conditions as described in CHAPTERS 1 and 2.

3-3. Results and Discussion

Fig. 3-1 shows the EPR spectra of NO-ferrous heme-PVP complex in DMF and MeOH, together with the spectrum of NO-ferrous-heme-pyridine (Fig. 3-1-(1)), where DMF and MeOH are poor and good solvents for PVP, respectively. The 9 lined hfs centered at g_2 can be seen as observed in CHAPTERS 1 and 2. In the DMF solution, as is shown in the expanded scale in the figure, the hfs of polymer system (Fig. 3-1-(2)) is rather unclear compared with that of ferrous heme-pyridine complex, which is, however, turned into distinct one, when the solvent was changed into MeOH (Fig. 3-1-(3)). The EPR spectra of NO-ferrous heme-PVP was found to be independent on the concentration of PVP. The alteration of the EPR spectra of Figs. 3-1-(2) and (3) does not originate from the difference of the solvent itself, since using pyridine or 4-ethylpyridine, the solvent effect on the EPR spectra is very

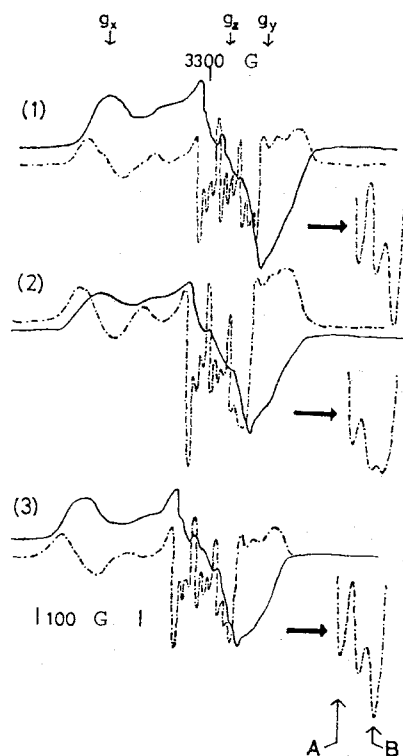


Fig. 3-1. The EPR absorption spectra of (1) NO-ferrous heme-pyridine in DMF, (2) NO-ferrous heme-PVP in DMF, and (3) NO-ferrous heme-PVP in MeOH. — First derivative, - - - - Second derivative.

small as compared with results of Figs. 3-1-(2) and -(3).

The absorption ratio arrowed as A and B is plotted against the volume fraction of MeOH, where the reduced viscosity is also included in the figure (Fig. 3-2). The hfs (B/A) changes continuously with the changes of the volume fraction of MeOH. From the data of the reduced viscosity, it can be said that when the polymer chain is extended, the hfs (B/A) becomes larger.

Similarly in Fig. 3-1, the ratio A to B in the spectra of Fig. 1-2 (CHAPTER 1) is plotted against the pK_a values of those pyridine derivatives. As shown in Fig. 3-3, the extent of the

hfs (B/A) is directly related to the basicity of nitrogen atom of each pyridine derivatives.

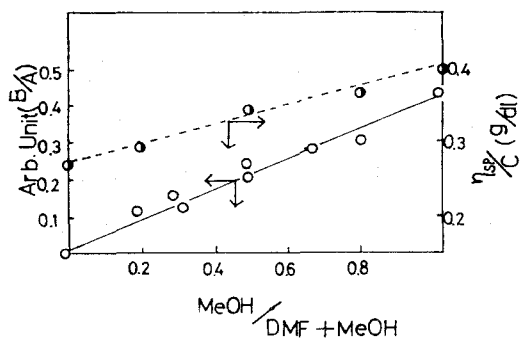


Fig. 3-2. Solvent effect on the hfs of EPR spectra of NO-ferrous heme-PVP.
 (o) The ratio of the absorption at A and B;
 (●) The reduced viscosity of PVP.

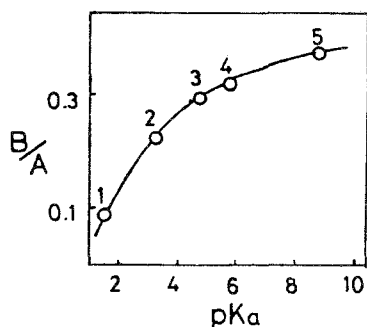


Fig. 3-3. The ratio of absorption at A and B in Fig. 1-2 is plotted against the pK_a of pyridine derivatives: 1. 4-cyanopyridine, 2. 4-acetylpyridine, 3. pyridine, 4. 4-methylpyridine, 5. 4-aminopyridine.

Here, the parameter of hfs (B/A) can be regarded as the degree of the delocalization of the unpaired electron on the 5th coordinated nitrogen base, since the linear relationship between the coupling constant and hfs (B/A) was observed experimentally. Therefore, it can be said that the increase of hfs (B/A) corresponds to delocalization of the electron on the nitrogen atom of the 5th ligand.

This shows that, in Fig. 3-3, the increase of basicity accompanies the increase of the spin-density on the nitrogen atom of pyridine ring.

The remarkable finding of this work is that the linkage between NO-ferrous iron-pyridine alters greatly within the polymer-ferrous heme complex. For example, as is seen in Fig. 3-2, the hfs (B/A) of PVP in DMF and MeOH are 0.05 and 0.4, respectively. These values may correspond to the extrapolated value of $pK_a = 0$ and $pK_a = 10$ of Fig. 3-3, which are obtained from relationship between pK_a and hfs (B/A). Thus the "apparent" basicity of nitrogen atom of pyridine in PVP seems to be changed more than 10 pK_a unit depending on the function of extension of polymer chain. Using pyridine itself, the solvent effect on the EPR spectra was examined, and hfs (B/A) was found to be 0.32 and 0.37 for DMF and MeOH, respectively, which is very small as compared with the polymer system (cf. Fig. 3-2). This suggests that there might exist the other factors affecting the EPR spectra, such as the polarity of heme-environment and the steric hindrance in the polymer chain. For example, the nearly identical values of hfs (B/A) in MeOH with both cases show that the NO-ferrous heme-pyridine linkage in PVP behaves as similar manner to monomeric system. With DMF, however, the fact that hfs (B/A) of PVP is much smaller value compared with that of pyridine itself, may suggest the absence of the interaction between the solvent and heme-moiety embedded in some peculiar polymer conformation.

In summary, the present method can provide the possibility to see directly the "event" occurred in the NO-ferrous heme-polymer system at the microscopic viewpoint.

3-4. References

- [1] T. Yonetani, H. Yamamoto, J. E. Erman, J. S. Leigh, and G. H. Reed, *J. Biol. Chem.*, 247, 2447 (1972).
- [2] H. Kon, *J. Biol. Chem.*, 243, 4350 (1968).
- [3] F. Taketa, W. E. Antholine, A. G. Mauk, and J. A. Libnock, *Biochemistry*, 14, 229 (1975).
- [4] H. Kon and N. Kataoka, *Biochemistry*, 8, 4757 (1969).
- [5] B. B. Wayland and L. W. Olson, *J. Am. Chem. Soc.*, 96, 6037 (1974).
- [6] M. Tamura, K. Kobayashi, and K. Hayashi, *Biochem. Biophys. Res. Commun.*, 70, 265 (1976).
- [7] K. Kobayashi, M. Tamura, and K. Hayashi, *Biochim. Biophys. Acta*, in press.
- [8] E. Tsuchida, K. Honda, and H. Sata, *Macromol. Chem.* 176, 2251 (1975).
- [9] E. Tsuchida, E. Hasegawa, and K. Honda, *Biochim. Biophys. Acta*, 427, 520 (1976).

CHAPTER 4. Flash Photolysis Studies on NO-Ferric Hemoproteins

4-1. Introduction

The photodissociability of various hemoproteins has been applied widely for the kinetic studies on ligand binding as the technique of flash photolysis [1-4]. For example, CO bound to the ferrous hemoprotein dissociates on illumination, and subsequently the recombination of CO to the ferrous hemoprotein occurs, as shown in Eq. (1).



Therefore, by the use of this technique, the kinetic studies of recombination of CO to the ferrous hemoproteins can be performed. The applicability of this method, however, seems to be limited to the ferrous ligated complexes, such as CO, O₂ and NO complexes, since it has been believed that only those ferrous complexes are photodissociable.

To extend this technique to the ferric state, the photodissociability of the various complexes of ferric hemoproteins have been examined.

4-2. Materials and Methods

HRP was purified from the crude material of Toyobo Co. by DEAE- and CM-cellulose column chromatography according to the method of Schannon et al. [5]. The crude material was dialyzed against 0.005 M Tris, pH 8.4, and was transferred to a DEAE-cellulose column previously equilibrated with the same buffer.

The fraction that was not absorbed by the column was isozymes B, C, D and E. The DEAE-cellulose column was then eluted with a linear gradient consisting of 500 ml of 0.005 M Tris, pH 8.4, and 500 ml of 0.005 M Tris, pH 8.4, containing 0.1 M NaCl. Effluent fractions were monitored at 280 nm for the estimation of protein content and 401 nm for the estimation of heme content. These fractions were purified by repeated chromatography on DEAE-cellulose until elution patterns indicated that each fraction was free from other HRP fractions. These fractions were isozymes A-1, A-2 and A-3. The fraction, which did not absorb to the DEAE-cellulose column, was dialyzed against 0.005 M acetate, pH 4.4, and transferred to a CM-cellulose chromatographic column previously equilibrated with the same buffer. The CM-cellulose column was then eluted with a linear gradient consisting of 500 ml of 0.005 M acetate, pH 4.4, and 500 ml of 0.1 M acetate, pH 4.4. These fractions were isozymes B and C. The five isozymes were tested for homogeneity by polyacrylamide disk electrophoresis. Each isozyme migrated as a single protein band with characteristic electrophoretic mobility. The enzymes used was the main fraction from the CM-cellulose column chromatography (isozyme C). The ratio of absorbance at 403 nm to that at 280 nm of this sample was 3.1.

The NO complexes of ferric hemoproteins in a cuvette (1 cm light path) for 20 min with occasional stirring.

The cuvette was evacuated and then NO gas was introduced to 1 atm. Optical absorption spectra were measured with a Cary-118 spectrometer. The concentration of HRP was determined spectrometrically by the use of an extinction coefficient at 403 nm of $107 \text{ mM}^{-1} \text{ cm}^{-1}$. The sample solution was photolyzed by the flash photolysis apparatus consisting of a xenon flash lamp, with a pulse width of 400 μs and an energy of 8 J, equipped with the optical detection system. Fluctuation of flash energy was less than 5 %. Temperature was thermostatically controlled at $20 \pm 0.1 \text{ }^\circ\text{C}$.

4-3. Results and Discussion

The optical absorption spectra of ferric and ferrous HRP complexes with NO are shown in Fig. 4-1. The NO-ferric HRP has the typical hemochromogen type spectrum with the absorption maxima at 565, 538 and 422 nm.

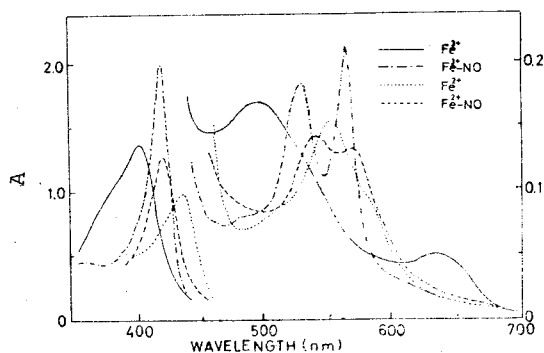


Fig. 4-1. Optical absorption spectra of ferric- and ferrous HRP and their complexes with NO. Ferrous HRP was obtained by the addition of small amounts of $\text{Na}_2\text{S}_2\text{O}_4$. Phosphate buffer (pH 7), 0.2 M.

Fig. 4-2 shows the time course of the absorption change after photolysis of NO-ferric HRP measured at different wavelengths. By photolysis the absorption at 405 nm, a characteristic to ferric HRP, increased and then decreased slowly with a half time of 1.7 ms. A similar time course of the absorption change was also seen at 425 nm, near the absorption maximum of NO-ferric HRP. The ferrous HRP, however, did not appear photolyzed, as shown by the absence of the absorption change at 435 nm. No absorption change at 412 nm was observed, where there is the isosbestic point between ferric HRP and its NO complex (cf. Fig. 4-1).

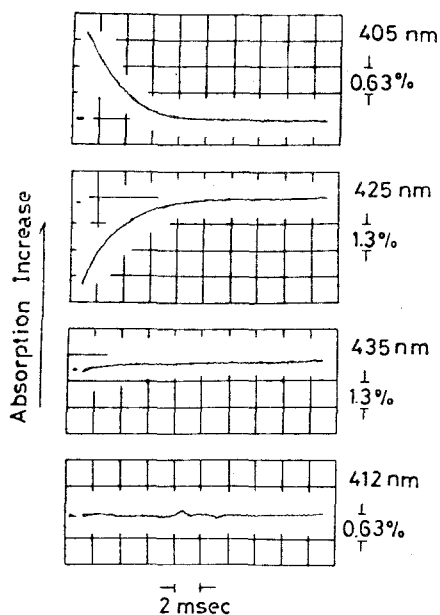


Fig. 4-2. The oscilloscope traces of absorption change by photolysis of NO-ferric HRP. Phosphate buffer (pH 7.4), 0.2 M.

The difference spectrum obtained at 1 ms after flash is shown in Fig. 4-3-(1). The spectrum has an absorption minimum at 422 nm and a broad peak around at 400 nm in the Soret region

together with distinct absorption minima at 538 and 568 nm, which is similar to the difference spectrum of NO-ferric HRP minus ferric HRP (solid line, Fig. 4-3-(2)). Therefore, it is concluded that the absorption changes in Fig. 4-2 are due to the photodissociation of the NO complex into the ferric state, followed by the recombination process of NO to ferric HRP, as shown in Eq. (2).

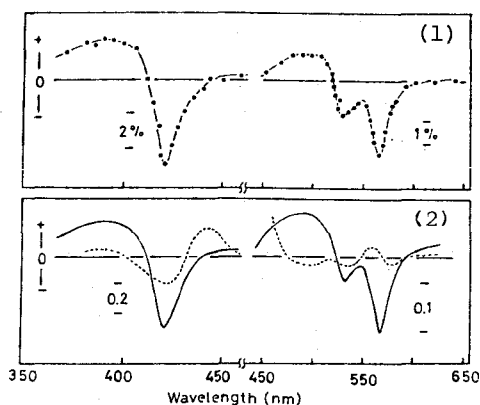


Fig. 4-3. (1) Kinetic difference spectrum of flash photolysis of NO-ferric HRP. The spectrum is taken at 1 ms after flash. (2) Difference spectra of NO-ferric HRP minus ferric HRP (—) and NO-ferrous HRP minus ferrous HRP (-----).

The recombination reaction of NO with ferric HRP obeys the pseudo first order kinetics because of the high concentration of NO. The second order rate constant is estimated to be $2 \times 10^5 \text{ M}^{-1} \text{ s}^{-1}$, which is pH-independent, in spite of the formation of the "alkaline" form of this enzyme above pH 11.

The present experiment demonstrates that the NO complex of ferric HRP is photodissociable. The product of the photodissociation is the ferric state, not the ferrous state. This is verified by the difference spectrum of Fig. 4-3. A similar photodissociation into the ferric state was also observed in other hemoproteins; the apparent photodissociability is in the order of

HRP \gg lactoperoxidase \approx Mb $>$ hemoglobin (Hb).

Here, the relatively low energy of flash lamp was used, because by this energy appreciable photodissociation of ferrous-NO complexes of these hemoproteins was not detected. This excluded the possibility of the photodissociation of ferrous-NO complexes formed in the sample, since NO reduces slowly the ferric state to the ferrous state. So far, in these experimental conditions the photodissociation of other ligand such as CN^- , N_3^- and F^- could not be observed.

It is noted that the optical absorption spectrum of NO-ferric HRP is a typical hemochromogen type, suggesting $\text{Fe}^{2+}\text{-NO}^+$ rather than $\text{Fe}^{3+}\text{-NO}$ for this complex. Taken this into consideration, a possible interpretation for the photodissociation is that the electronic structure of NO-ferric HRP is similar to that of the photodissociable ferrous complex, such as a CO complex. In any case, the photodissociation of NO-ferric hemoproteins into ferric state may give the critical argument concerning the quantum mechanical interpretation of this phenomenon [6].

The ability of the photodissociation of NO complexes into the ferric state can provide a unique approach to the kinetic

studies of ligand-binding. These are described in CHAPTER 5.

4-4. References

- [1] Q. H. Gibson, *Biochem. J.*, 71, 293 (1959).
- [2] C. A. Sawicki and Q. H. Gibson, *J. Biol. Chem.*, 251, 1533 (1976).
- [3] B. Chance and M. Erecinska, *Arch. Biochem. Biophys.*, 141, 675 (1971).
- [4] D. Kertesz, E. Antonini, M. Brunori, J. Wyman, and R. Sito, *Biochemistry*, 4, 2672 (1965).
- [5] L. M. Schannon, E. Kay, and J. Y. Lew, *J. Biol. Chem.*, 241, 2166 (1966).
- [6] T. Kitagawa, Y. Kyogoku, T. Iizuka and M. Saito, *J. Am. Chem. Soc.*, 98, 5169 (1976).

CHAPTER 5. Kinetic Analysis of the Recombination of NO with Ferric Hemoproteins by the Flash Photolysis Method

5-1. Introduction

The process after photodissociation of the ferrous ligated hemoproteins has been established [1]. The photodissociated product is the ferrous unligated state and subsequently the photodissociated ligand recombines with this ferrous heme. In this case, the rate constants for recombination of the ligand with the ferrous hemoproteins obtained by the flash photolysis and the stopped flow methods are identical with each other except CO-Hb [2]. In contrast to the ferrous state, the photodissociation of the ferric state is more complex. This comes from the fact that the water molecule occupies the 6th position in the ferric unligated state in contrast to the vacancy at this position in the ferrous unligated state. The following processes can be anticipated after photodissociation of NO-ferric hemoproteins; (1) the formation of the pentacoordinated heme, (2) the competitive ligand binding of NO and water molecule with the pentacoordinated heme. This chapter describes kinetic experiments on the flash photolysis of NO-ferric hemoproteins at room temperature, of which results are compared with those obtained by stopped flow experiments.

5-2. Materials and Methods

Sperm whale Mb was prepared in the same manner as described in CHAPTER 2 [3]. Ferric Mb was obtained from the oxyform by the treatment of ferricyanide, followed by DEAE-cellulose column chromatography. HRP was purified in the same manner as described in CHAPTER 4 [4]. The isozymes used in this study were HRP-A and HRP-C according to the classification of Paul [5] and Schannon [4]. The NO complexes of ferric hemoproteins were prepared by two methods. In one method, nitrogen gas was passed over the surface of solution of ferric hemoproteins in a small cuvette for 20 min with occasional stirring. The cuvette was evacuated, and then 1 atom of NO gas was introduced anaerobically. In other method, a solution of 0.1 M phosphate buffer (pH 6-8), 0.1 M Tris-HCl (pH 8-10) or 0.1 M glycine-NaOH (above pH 10) was deaerated by extensive flushing with nitrogen, and then was bubbled NO gas anaerobically for at least 20 min. A small volume of the concentrated hemoproteins were separately deoxygenated by repeated evacuation and flushing with nitrogen and added to the NO saturated buffer solution. The concentration of NO in the solution was adjusted by mixing NO and N₂ saturated buffer solutions. The value of 2 mM was used for the saturated NO solution. Optical absorption spectra were measured with a Cary-118 spectrometer.

The photolysis experiments were carried out as previously described in CHAPTER 4 [6]. The stopped flow apparatus used was a Union Giken spectrometer model RA-401. A solution of ferric hemoprotein, which was prepared by careful equilibration with nitrogen gas, was introduced into one of the reservoirs of the flow system.

5-3. Results

5-3-1. NO-ferric Mb

Fig. 5-1 shows time course of the absorption change at different wavelengths after photolysis of NO-ferric Mb at pH 6. By photolysis, the absorption at 403 nm, characteristic to acid-ferric Mb, jumped and then decreased with a half time of 7 ms. A similar time course of absorption change was also seen at 420 nm, which is nearly an absorption maximum of NO-ferric Mb.

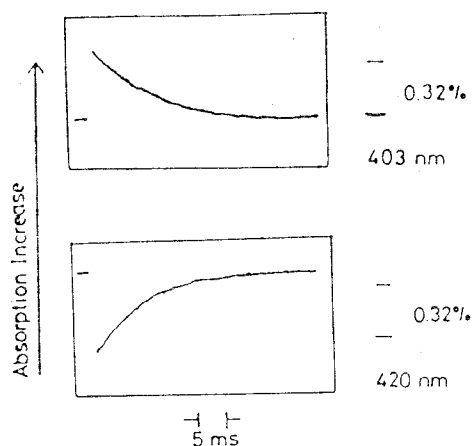


Fig. 5-1. The oscilloscope traces of the absorption change by photolysis of NO-ferric Mb. Phosphate buffer (pH 6), 0.1 M.

Fig. 5-2-(1) shows the kinetic difference spectra in the Soret region obtained 1 ms after flash at different pHs. For comparison, the corresponding difference spectra of NO-ferric Mb minus ferric Mb are shown in Fig. 5-2-(2). At pH 6, the kinetic difference spectrum has an absorption minimum at 420 nm and a broad peak around 400 nm, and is similar to the difference spectrum of NO-ferric Mb minus ferric Mb at pH 6. Similarly, the kinetic difference spectrum at pH 10 equals that of NO-ferric Mb minus

its alkaline form. The kinetic difference spectrum at pH 8.5 is intermediate between the two. The isosbestic point of 417 nm seen in Fig. 5-2-(1) corresponds with that between acid- and alkaline-forms of ferric Mb (cf. Fig. 5-2-(2)). This indicates that the acid and alkaline forms or a mixture of the two forms of ferric Mb appeared at 1 ms after photolysis. Therefore, it is concluded that the absorption change in Fig. 5-1 is due to photodissociation of the NO complex into the ferric Mb and NO, followed by the recombination process.

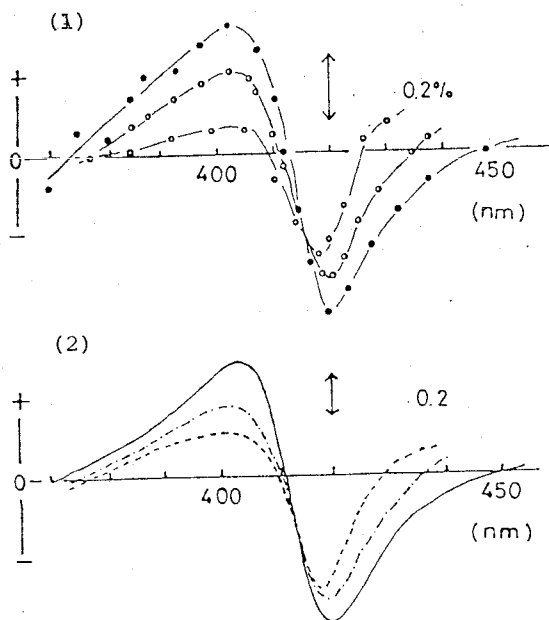


Fig. 5-2. (1) Kinetic difference spectra of flash photolysis of NO-ferric Mb in the Soret region. The spectra were taken at 1 ms after flash. (●) Phosphate buffer (pH 6), 0.1 M (●) Tris-HCl (pH 8.5), 0.1 M, and (○) glycine-NaOH (pH 10), 0.1 M. (2) Difference spectra of NO-ferric Mb minus ferric Mb at pH 6 (—), 8.5 (---), and pH 10 (· · ·).

The recombination reaction of NO with ferric Mb obeys the pseudo first order kinetics in the whole pH range (inset of Fig. 5-3) because of the high concentration of NO. This shows that equilibrium is practically attained between the acid- and alkaline-forms at pH 8.4 and 9 during the recombination process. Fig. 5-3 shows the pH dependence of the rate constants for the recombination of NO with ferric Mb obtained by the flash photolysis and the stopped flow methods. The rate constants obtained are not different between the two methods in the whole pH range (pH 6-10.5). The values decrease with the increase of pH and its pH dependence gives a pK value of 8.3. This corresponds to the pK value for the acid-alkaline transition of ferric Mb. From the figure, the second order rate constants for NO binding to the acid- and alkaline-forms of ferric Mb are calculated at 5×10^4 and $1.5 \times 10^4 \text{ M}^{-1}\text{s}^{-1}$, respectively.

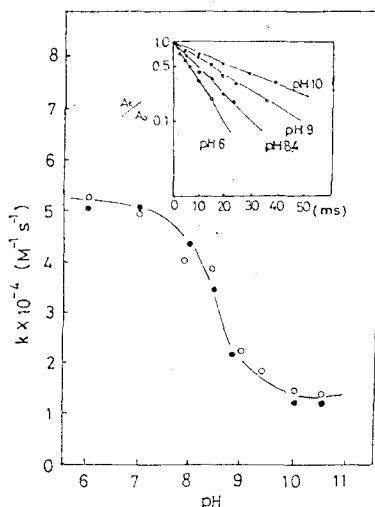


Fig. 5-3. pH dependence of the rate constants of recombination with ferric Mb. (●) Stopped flow method; (o) flash photolysis method. Inset, First order plots of the absorption change at 403 nm by flash photolysis at different pHs.

5-3-2. NO-ferric HRP-C

Fig. 5-4 shows pH dependence of the rate constants for the recombination of NO with ferric HRP-C obtained by flash photolysis and stopped flow experiments. The rate constants obtained by the two methods are identical ($1.9 \times 10^5 \text{ M}^{-1} \text{ s}^{-1}$) in the pH range between 5 and 9. Above pH 9, however, the values determined by stopped flow method decrease with the increase of pH, giving a pK value of 10.8. This value corresponds to the pK value for acid-alkaline transition of this enzyme. On the other hand, the values determined by the flash photolysis remain constant until pH 11.8. This shows that the ferric enzyme which appeared immediately after photolysis differs from the alkaline form at above pH 8, recombining with NO at the same velocity as with the acid form.

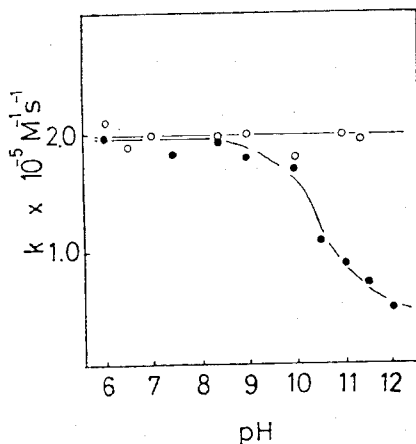


Fig. 5-4. pH dependence of the recombination rate constants of NO with ferric HRP-C. The data obtained by the flash photolysis (o) and the stopped flow (●) methods are plotted against pH.

This is consistent with the fact that the kinetic difference spectra by flash photolysis at alkaline pHs are identical to those

at neutral and acidic pHs, and are assigned to the difference spectrum of NO-ferric minus the acid form, but not the alkaline form, as shown in Fig. 5-5.

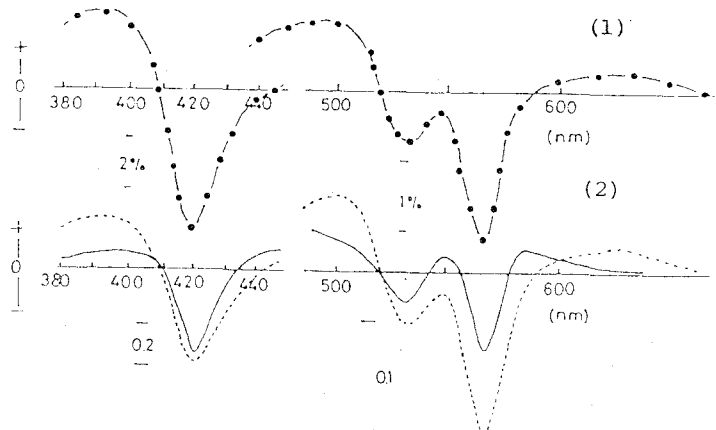


Fig. 5-5, (1) Kinetic difference spectrum of flash photolysis of NO-ferric HRP-C at pH 11.5. The spectrum is taken at 1 ms after flash. Glycine-NaOH (pH 11.5), 0.1 M. (2) Difference spectra of NO-ferric HRP-C minus ferric HRP-C at pH 6 (—) and pH 11.5 (---).

5-3-3. NO-ferric HRP-A

Ferric HRP-A has a pK value of 8.4 for acid-alkaline transition. The time course of the absorption change at 420 nm after photolysis is shown in inset of Fig. 5-6. The absorption change at pH 6 obeys the first order kinetics, from which the second order rate constant for the NO recombination is estimated to be $2.0 \times 10^5 \text{ M}^{-1} \text{ s}^{-1}$. Above pH 9.4, however, the absorption change after photolysis deviates from the first order kinetics and consists of fast and slow phases (Fig. 5-6). The time resolved kinetic difference spectra after photolysis at pH 6 and 10 are shown in Fig. 5-7. The spectra obtained at pH 6 have the

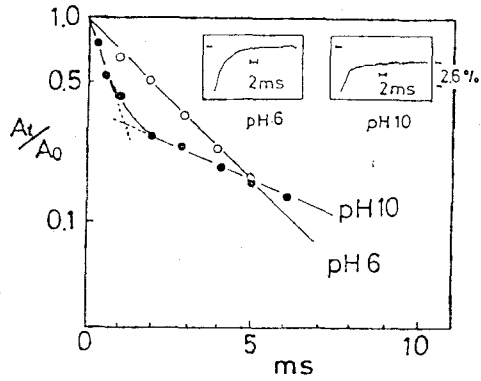


Fig. 5-6. First order plots of absorption change at 420 nm from the traces of inset of Fig. 5-6. Inset. The oscilloscope traces of the absorption change after photolysis of NO-ferric HRP-A. Phosphate buffer (pH 6), 0.1 M, and glycine-NaOH (pH 10), 0.1 M.

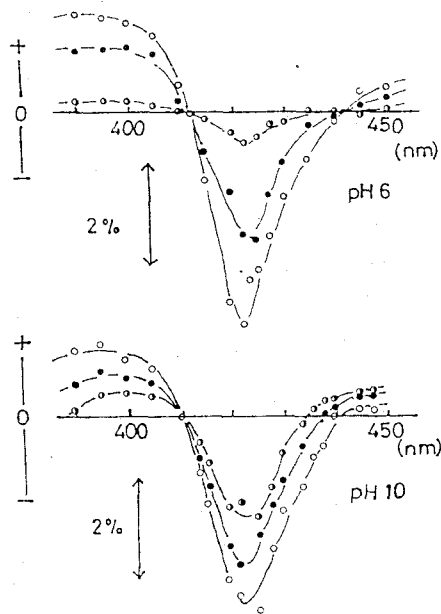


Fig. 5-7. Kinetic difference spectra of flash photolysis of NO-ferric HRP-A at pH 6 and pH 10. The spectra were taken at 1 ms (o), 2 ms (●) and 5 ms (◐) after flash, respectively.

isosbestic points at 413 and 441 nm, and resembles that of NO-ferric HRP-A minus acid-ferric HRP-A. Thus, absorption change at pH 6 (inset of Fig. 5-6) is concluded to reflect the recombination of NO with acid-ferric HRP-A. At pH 10, the spectra at 2 and 5 ms do not give an isosbestic point at 441 nm. At pH 6, the absorbance at 441 nm remained unchanged, but at pH 10, it increased with a half time of 2 ms and then decreased slowly (Fig. 5-8-(1)).

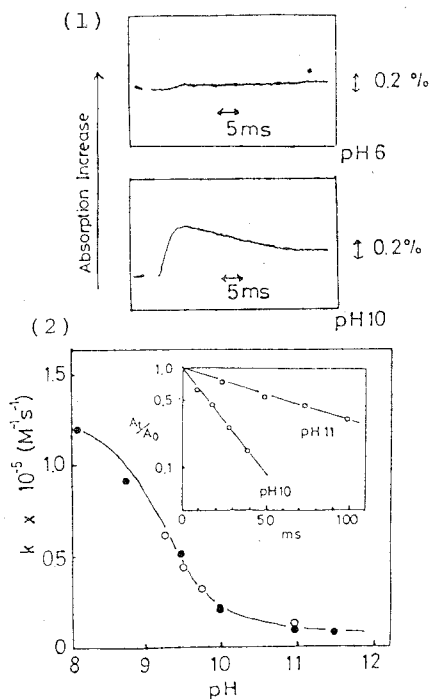
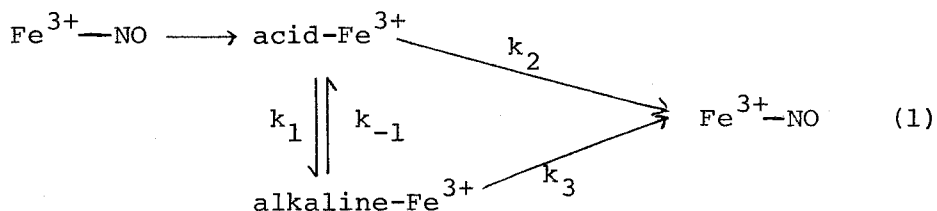


Fig. 5-8. (1) The oscilloscope traces of absorption change at 441 nm by photolysis of NO-ferric HRP-A. (2) pH-dependence of the rate constants recombination of NO with ferric HRP-A. (●) Stopped flow method, (○) Flash photolysis method. Inset: First order plots of absorption change in the slow process of Fig. 5-8-(1).

The increase of the absorption at 441 nm is attributable to the formation of alkaline-form during the reaction (cf. Fig. 5-5). The slow decrease obeys the first order kinetics, as shown in inset of Fig. 5-8-(1). Assuming that this absorption change represents the recombination of NO with the alkaline form of ferric HRP-A, the rate constant can be calculated. Fig. 5-8-(2) shows pH dependence of the value obtained by the above procedure and the flow method. This indicates that the slow process is due to the recombination of NO and the alkaline form of ferric HRP-A. The fast phase seen in Fig. 5-8-(1) thus is concluded to involve acid-alkaline transition and recombination of NO with the acid form. The disappearance of acid-ferric HRP-A was followed at 432 nm, an isosbestic point between alkaline-ferric HRP-A and NO-ferric HRP-A. This absorption change obeys the first order kinetics in the whole pH-range as shown in Fig. 5-9-(1). The reaction paths is schematized as follows:



Assuming that k_{-1} and k_3 are much smaller than k_1 and k_2 , the rate constant of the disappearance of acid form is expressed by Eq. (2):

$$- \frac{d[\text{Acid form}]}{dt} = \{k_2[\text{NO}] + k_{-1}\}[\text{Acid form}] \quad (2)$$

where k_2 is the rate constant for the recombination of NO with

acid form and k_1 is the rate constant for the conversion from the acid form to the alkaline form. The apparent first order rate constant (k_{app}) in Fig. 5-9-(1) can be expressed as

$$k_{app} = k_2[\text{NO}] + k_1 \quad (3)$$

Fig. 5-9-(2) shows the dependence of k_{app} upon the concentration of NO at different pH, giving straight lines. From the slope and intercept in Fig. 5-9, k_2 and k_1 can be estimated. Here the k_2 values are almost constant within experimental error, which supports the reasonable basis of Eq. (3). Eq. (3) in the NO

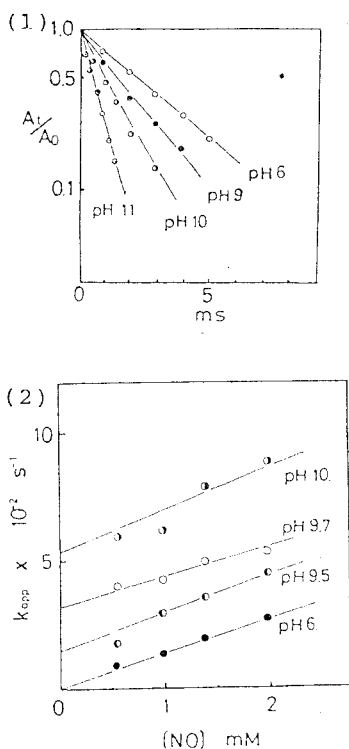


Fig. 5-9. (1) First order plots of absorption change at 432 nm by photolysis of NO-ferric HRP-A. (2) The correlation between the concentration [NO] and the first order rate constant determined at 432 nm.

saturated solution becomes $k_{app} = 4 \times 10^5 \text{ s}^{-1} - k_1$ of ferric HRP-A and $k_{app} = 3.8 \times 10^5 \text{ s}^{-1} - k_1$ of ferric HRP-C. From these equation, k_1 values were calculated. The k_1 values of ferric HRP-A and -C increased with the increase of pH. The plot of k_1 vs. $[\text{OH}^-]$ exhibits a linear relationship as shown in Fig. 5-10.

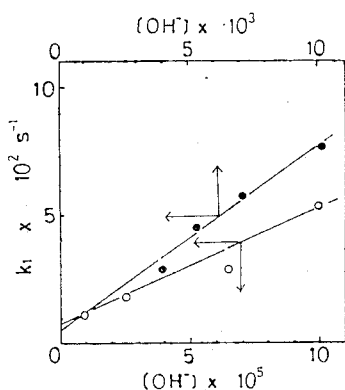


Fig. 5-10. k_1 vs. pH plot in the acid-alkaline conversion of ferric HRP-A (○) and HRP-C (●)

5-4. Discussion

Photodissociation of NO complexes into the ferric state can provide a unique approach for the kinetic studies of ligand binding. The typical examples are shown in Fig. 5-2 and 5-3. The reaction scheme is proposed in Fig. 5-11. The water molecule is taken up into the pentacoordinated form within 1 ms after dissociation of NO by photolysis. This is confirmed by the fact that the kinetic difference spectrum is identical with that of acid-ferric Mb. This shows that the coordination of H_2O to the pentacoordinated ferric Mb is much faster than the recombination of NO with ferric Mb. If the half time of the coordination

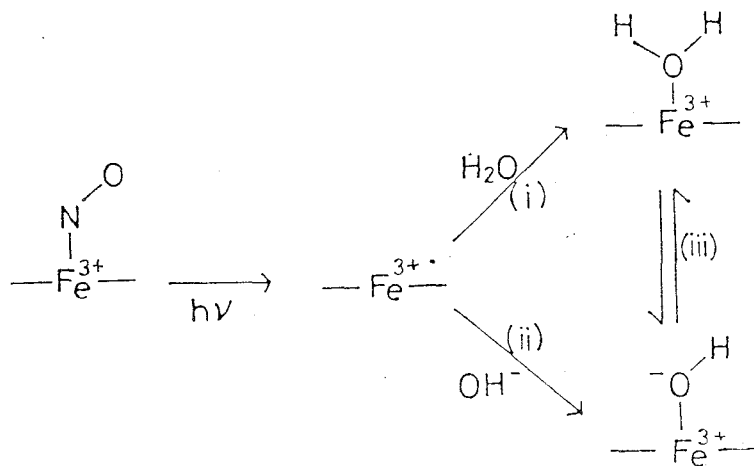


Fig. 5-11. Schematic presentation after photodissociation of NO-ferric Mb.

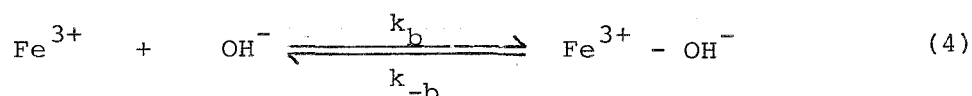
of water molecule is less than 100 μs , the rate constant of coordination of H_2O is greater than $10^2 \text{ M}^{-1} \text{ s}^{-1}$.

The formation of alkaline form is also much faster than the recombination of NO with ferric Mb. The alternative pathways for the formation of the alkaline form after photolysis are shown in Fig. 5-11. First, a water molecule is taken up into pentacoordinated form to yield the acid form, and then the water molecule dissociates a proton to form the alkaline form. Second, the direct coordination of a hydroxylate ion occurs at the 6th position of the pentacoordinated form. At the moment, these two pathways cannot be discriminated. The proton transfer in the acid-alkaline transition (iii) is very fast, i.e., in the order of 10^6 s^{-1} . If the reaction occurs via path (i), the rate constant should be larger than $10^6 \text{ M}^{-1} \text{ s}^{-1}$.

The present results demonstrate that unlike ferric Mb the conformation of ferric HRP which appeared after photolysis of NO-ferric HRP is identical with the acid form of ferric HRP in the whole pH range. This is verified by the kinetic difference spectra and by recombination rate of NO with the enzyme. The deviation from first order kinetics in the NO recombination at pH 10 can be explained in terms of the competition between the NO recombination with the acid form and the transformation from the acid form to the alkaline form. The rate constant for the formation of the alkaline form calculated from Eq. (3) agrees with the values obtained from the acid-alkaline transition of ferric HRP-C and -A [7-9]. Morishima et al. [10] have suggested that this slow rate is ascribed to the direct exchange of the 6th ligand on the ferric heme. It is obvious, however, that the slow rate of alkaline ionization does not necessarily mean an involvement of a conformational change. If an amino acid residue deprotonates in alkaline solution with a conformational change in the protein, a saturation effect should be observed as the hydroxide ion concentration increases. Such a saturation effect was not observed, and the rate increased exponentially with the increase of pH in Fig. 5-10. Similar values for the acid-alkaline conversion were obtained by the pH jump method by Araiso et al. [7], who proposed that this process is due to abstracting a hydrogen ion from the ligand water molecule, and the slow rate was explained by assuming that a strong hydrogen bond interaction between the dissociable proton of the water molecule at the 6th position and distal base occurs.

The results shown in Fig. 5-10 might be explained by this mechanism, but this proposal is based on the assumption that H₂O coordinates at the 6th position of the acid form of ferric HRP.

In next chapter [11], it is proposed that acid-ferric HRP holds a pentacoordinated structure. Therefore, the formation of the alkaline form of ferric HRP should be explained simply by the direct coordination of OH⁻ at the 6th position, which is vacant at acidic and neutral pHs, as shown in Eq. (4).



The values of k_b and k_{-b} are $6.8 \times 10^5 \text{ M}^{-1}\text{s}^{-1}$ and 65 s^{-1} for ferric HRP-A and $7.3 \times 10^4 \text{ M}^{-1}\text{s}^{-1}$ and 46 s^{-1} for ferric HRP-C, respectively (Fig. 5-10). So far, examination by laser photolysis revealed that the difference spectrum appearing 100 ns after photodissociation of NO-ferric HRP was indistinguishable from that of the native enzyme. There was no appreciable spectral indication suggesting the presence of intermediates at any wavelengths in this time scale. Therefore, even if a water molecule coordinates at the 6th position of ferric HRP, the recombination of a water molecule occurs in less than 100 ns.

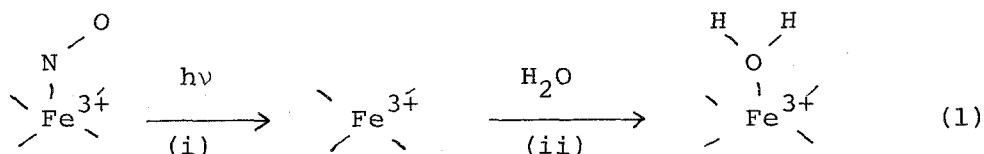
5-5. References

- [1] E. Antonini, M. Brunori, "Hemoglobin and Myoglobin in Their Reactions with Ligands", North-Holland Publ. Co., Amsterdam and London (1971).
- [2] C. A. Sawicki, Q. H. Gibson, *J. Biol. Chem.*, 251, 1533 (1976).
- [3] I. Yamazaki, K. Yokota, and K. Shikama, *J. Biol. Chem.*, 239, 4151 (1964).
- [4] L. M. Schannon, E. Kay, and T. Y. Lew, *J. Biol. Chem.*, 241, 2166 (1966).
- [5] K. G. Paul, *Acta Chem. Scad.*, 12, 1312 (1967).
- [6] M. Tamura, K. Kobayashi, and K. Hayashi, *FEBS Lett.*, 88, 124 (1978).
- [7] T. Araiso and I. Yamazaki, *Biochemistry*, 17, 942 (1978).
- [8] N. Epstein and A. Schejter, *FEBS Lett.*, 25, 46 (1972).
- [9] H. Kihara, S. Saigo, T. Iizuka, and Y. Ishimura, *Biochim. Biophys. Acta*, 533, 112 (1978).
- [10] I. Morishima, S. Ogawa, J. Inubushi, T. Yonezawa, and T. Iizuka, *Biochemistry*, 16, 5109 (1977).
- [11] K. Kobayashi, M. Tamura, K. Hayashi, H. Hori, and H. Morimoto, *J. Biol. Chem.*, 255, 2239 (1980).

CHAPTER 6. Electron Paramagnetic Resonance and Optical Absorption
Spectrum of the Pentacoordinated Ferric Hemoproteins

6-1. Introduction

Except for certain M-type abnormal Hb, the penta-coordinated form of the ferric state of hemoproteins has not yet been realized. This comes from the fact that the water molecule occupies the 6th position in the ferric unligated state in contrast to the vacancy at this position in the ferrous unligated state [2]. The recent discovery of the photodissociability of NO-ferric hemoprotein complexes [3,4] has opened up the possibility of observing such a pentacoordinated form of the ferric state. It seemed possible that this might appear after departure of NO by photolysis (i), prior to the coordination of a water molecule (ii) at the 6th position, as shown in Eq. (1).



NO-ferric-complex pentacoordinated native-aquao-form

In CHAPTER 5, it was shown that the water molecule coordinates to the ferric pentacoordinated Mb within 1 ms after photodissociation of NO (the step (ii) of Eq. (1)). At cryogenic temperatures the step (ii) does not occur. Thus, the photolysis of NO-ferric hemoproteins at liquid helium temperature (4.2 K) was performed, in order to generate and trap the pentacoordinated form. Optical and EPR characteristics of this form are given in this chapter.

6-2. Materials and Methods

HRP and Mb were purified as previously described [5, 6]. HRP used (RZ = 3.2) was a main fraction absorbed on the CM-cellulose column, which was a mixture of isozymes B and C according to the nomenclature of Schannon et al. [6].

The NO complexes of ferric hemoproteins were prepared as previously described in CHAPTER 5. The NO-complexes thus formed were anaerobically injected into EPR sample tubes with 0.5 mm inner diameter and frozen rapidly with liquid nitrogen. EPR absorption spectra were measured with Varian E-line and JEOL ME-2X spectrometers, both of which were operated with X-band 100 KHz-field modulation units. The photodissociation experiments were performed by illuminating the sample by a 300 W tungsten lamp for 10 min through a window in the EPR cavity at liquid helium temperature. The spectra of the photolyzed products were measured after cessation of the illumination. All the measurements were performed at liquid helium temperature (4.2 K) except otherwise noticed according to the method of Nagai et al. [7].

Optical absorption spectra at liquid helium temperature were measured with a Shimazu D-40 DFS spectrometer as described by Iizuka et al. [8]. The sample solution (NO-ferric hemoproteins) was transferred into a twin optical cuvette assembly held in an inner Dewar flask filled with liquid nitrogen, and frozen quickly. After precooling the inner Dewar, liquid nitrogen was removed and then liquid helium was transferred into the inner

Dewar flask. The photolysis was performed by illuminating the optical cuvette through the window of the Dewar flask with the 300 W tungsten lamp for 10 min, in a similar manner to that of EPR measurement.

The NO complexes of ferric hemoproteins are relatively unstable and transformed gradually to the corresponding ferrous complexes. Thus special care must be taken during the course of sample preparation to avoid the formation of ferrous NO complexes, which interfere strongly both EPR and optical analyses. The absence of the NO-ferrous hemoprotein complexes in the sample was checked by EPR measurements in the $g = 2$ region where NO-ferrous complexes have intense signals [9].

Ferric Mb was crystallized and grown in an 80 % saturated ammonium sulfate solution at pH 6. One single crystal of ferric Mb was placed in the bottom of a quartz sample tube with a small quantity of mother liquid and the sample tube. Air in the sample tube was removed by repeating gentle evacuation and flushing with nitrogen gas. NO gas was injected into this sample tube and the sample was kept for several hours at 4°C. The sample was frozen in liquid nitrogen and then cooled down to liquid helium temperature. The Dewar flask filled with liquid helium was inserted into the cavity, and the sample tube with the crystal was placed in the center of the Dewar flask. The sample tube mounted with the crystal was rotated around its crystal axis by hand at 10° intervals. The illumination was performed through the window of the cavity. The magnetic field strength was determined by the nuclear magnetic field resonance of protons in water.

6-3. Results

6-3-1. Optical study

Fig. 6-1 shows the optical absorption spectra of acid-ferric Mb, NO-ferric Mb and its photodissociated product measured at 4.2 K. On illumination with a 300 W tungsten lamp, the absorptions around 650, 500 and 400 nm characteristic to the ferric high-spin state appeared with concomitant decrease of the hemochromogen type spectrum of NO-ferric Mb. The broad absorption from 600 to 680 nm of the photodissociated product does not possess the twin peaks at 625 and 640 nm of native acid

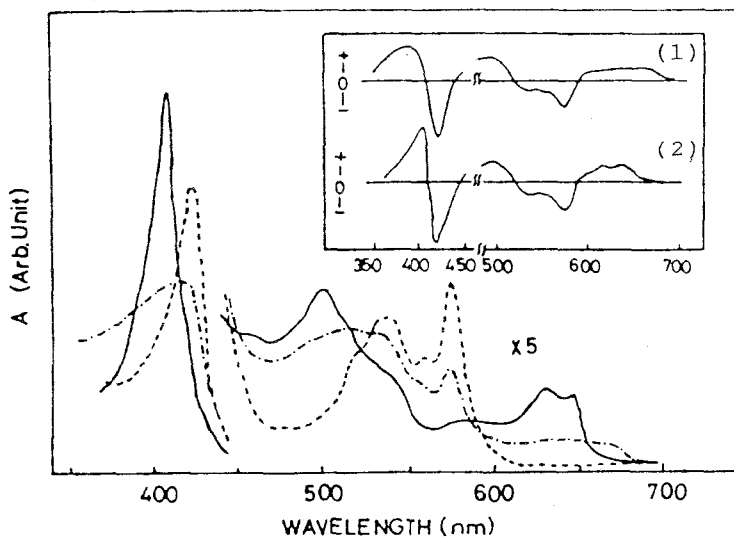


Fig. 6-1. Optical absorption spectra of acid-ferric Mb (—), NO-ferric Mb (---), and its photodissociated product (-·-·-) measured at liquid helium temperature. bis-Tris buffer (pH 6), 0.2 M. Inset. (1) Difference spectrum before and after illumination of NO-ferric Mb at pH 6. (2) Difference spectrum of NO-ferric Mb minus ferric Mb.

ferric Mb, which are assigned to the charge transfer bands due to the 6th coordination with a water molecule [10].

The absorption change caused by illumination was saturated almost at half-way to complete photodissociation and more than 20 min illumination caused no further change in the spectrum observed in Fig. 6-1. In the inset of Fig. 6-1 the difference spectrum caused by the illumination of NO-ferric Mb (1) is compared with that between NO-ferric Mb and ferric Mb (2). Spectrum (1) has a broad absorption maximum at 380 nm and a broad absorption from 600 to 680 nm, while spectrum (2) has a maximum at 408 nm and twin peaks around 650 nm, which are also seen in the absolute spectrum of native ferric Mb.

Fig. 6-2 shows results obtained from similar experiments on ferric HRP. On illumination, the high spin absorption bands around 400, 490 and 640 nm appeared. The difference spectrum of ferric HRP before and after illumination, shown in inset (1) of Fig. 6-2, is indistinguishable from that of NO-ferric HRP minus native acid-ferric HRP at pH 6 (inset (2), Fig. 6-2). The absorption spectrum of the photodissociated product obtained at pH 11.5, where the photodissociation occurred to a greater extent, is identical to that at pH 6.

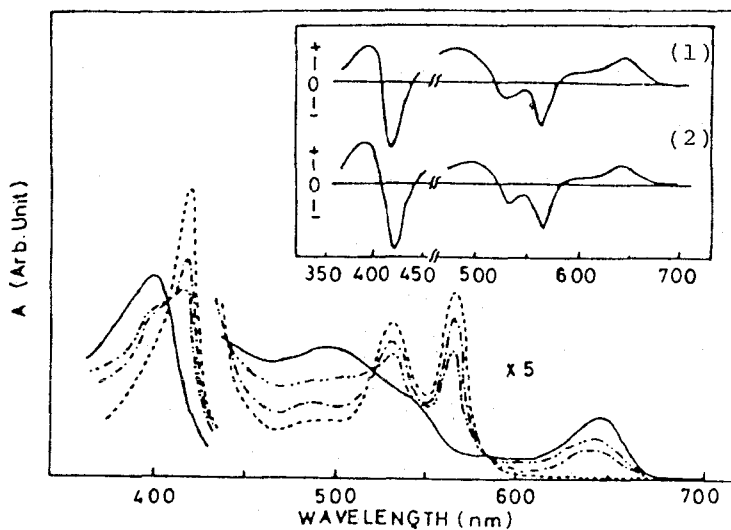


Fig. 6-2. Optical absorption spectra of ferric HRP (—), NO-ferric HRP (---), and its photodissociated product at pH 6 (-.-.-) and pH 11.5 (-.-.-.-) measured at liquid helium temperature. bis-Tris buffer (pH 6), 0.2 M, and glycine-NaOH buffer (pH 11.5), 0.2 M. The spectrum of the photodissociated product at pH 11.5 was normalized against the spectrum of NO-ferric HRP at pH 6. Inset. (1) Difference spectrum before and after illumination of light at pH 6. (2) Difference spectrum of NO-ferric HRP minus ferric HRP at pH 6.

6-3-2. EPR absorption

The EPR spectra of acid-ferric Mb and photodissociated product of NO-ferric Mb are compared in Fig. 6-3. Since NO-ferric Mb is diamagnetic, the EPR spectrum is flat before illumination. On illumination, a broad absorption having the g value of 5.8 appeared, which differs clearly from that of native acid-ferric Mb at $g = 6.0$ (Fig. 6-3-(2)). A very broad absorption appeared in the range from $g = 4$ to 2. When the sample was photolyzed at pH 10, a similar $g = 5.8$ absorption appeared, but the low spin type EPR signal due to its alkaline form did not.

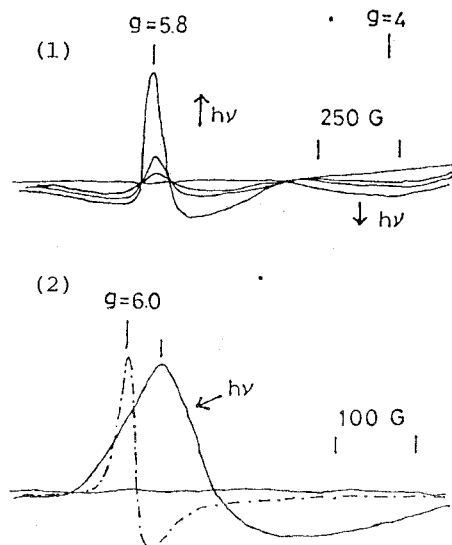


Fig. 6-3, (1) The change of EPR signal from NO-ferric Mb to its photolyzed product by successive illumination. The spectra are taken at 0 min, 1 min, 5 min, 30 min, after illumination started. bis-Tris (pH 6), 0.2 M
 (2) Comparison of the EPR absorption spectra of ferric Mb at pH 6 (---) and the photodissociated product of NO-ferric Mb after 10 min illumination (—).

Fig. 6-4 shows the angular dependency of the g value of the photodissociated product together with the acid-ferric Mb measured with the single crystal. Fig. 6-4-(1) shows the appearance of the $g = 5.8$ signal by illumination of the crystal of ferric Mb with the ab -plane parallel to the direction of magnetic field. The adjacent strong $g = 6.0$ signal is ascribable to native acid-ferric Mb presented in the crystal. Fig. 6-4-(2) shows the appearance of the $g = 2.9$ signal at an appropriate orientation in ac -plane of the crystal. When the crystal was rotated in the ab -plane, for example, both signals

at $g = 5.8$ of the photodissociated product and at $g = 6.0$ of acid-ferric Mb behave similarly against the degree of the rotation of the crystal (Fig. 6-4-(4)).

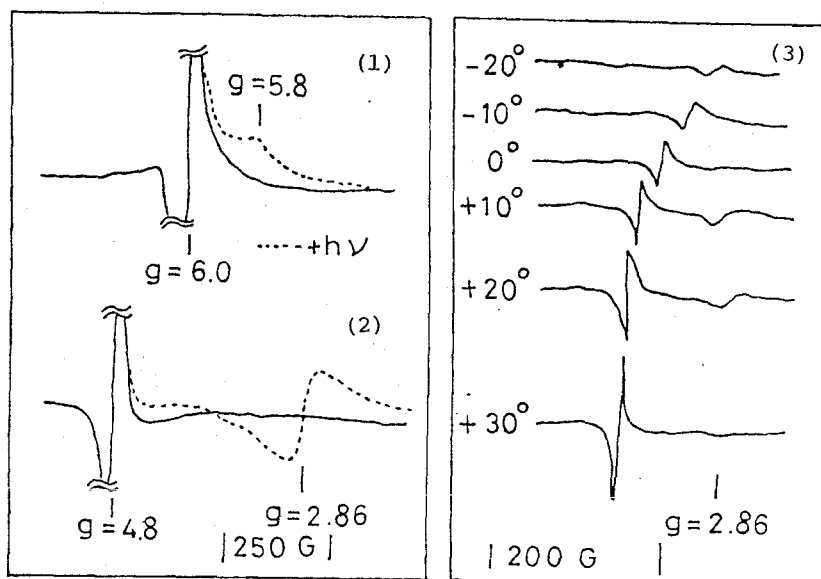


Fig. 6-4. Appearance of the EPR signal of the photolyzed product measured with a single crystal of NO-ferric Mb at 4.2 K. The dotted line was obtained after 10 min of illumination at 4.2 K. The solid line shows the EPR signal of native ferric Mb in the single crystal, which did not combine with NO. The ab-plane is parallel to the direction of the magnetic field in (1) and the ac-plane in (2). (3) Angular dependent changes of the EPR spectra of the single crystal of NO-ferric Mb after 10 min of illumination. The signal with $g = 2.86$ was seen at 10° and 20° of rotation of ac-plane. (2) corresponds to the spectrum at 20° .

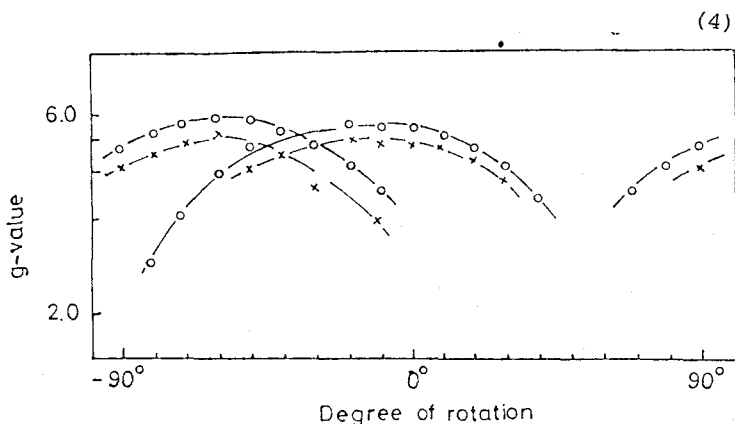


Fig. 6-4. (4) Angular dependence of the g tensor of the photolyzed product (x-x) and native ferric Mb (o-o). The crystal was rotated in the ab -plane.

EPR measurements have also been performed with the photodissociated product of NO-ferric HRP (Fig. 6-5). As is seen in Fig. 6-5-(1), on illumination a broad EPR signal appeared at $g = 3.06$, whereas no EPR signal was detected in the $g = 6.0$ region. When the temperature of the sample was increased to 77 K and then decreased again to 4.2 K, the broad $g = 3$ signal decreased with concomitant appearance of high spin signal of the doublet at $g = 6$ formed by elevating the temperature to 77 K is the same as that of ferric HRP at pH 6, as shown in Fig. 6-5-(3). Similar results were also obtained at pH 11.5.

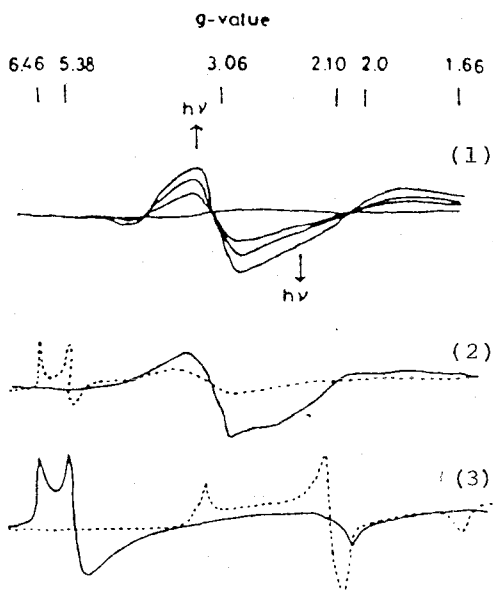


Fig. 6-5. (1) The changes of the EPR signal from NO-ferric HRP to its photolyzed product by successive illumination of light. The spectra are taken at 0 min, 2 min, 5 min, and 20 min after illumination started. bis-Tris (pH 6), 0.2 M. (2) Effect of temperature on the EPR spectra of the photolyzed product of NO-ferric HRP. The dotted line was obtained by the following procedure: the photolyzed sample at 4.2 K (solid line) was dipped into a Dewar filled with liquid nitrogen for a few minutes and then cooled again to 4.2 K, at which temperature the measurement was made. (3) EPR absorption spectra of native ferric HRP at pH 6 (—) and 11.5 (····) at 4.2 K. Glycine-NaOH buffer (pH 11.5), 0.2 M.

6-4. Discussion

The pentacoordinated state of ferric Mb is successfully trapped at 4.2 K by the photolysis of NO-ferric Mb. The most characteristic feature of this state is its broad absorption maximum at 380 nm in the Soret region. The iron atom in this pentacoordinated high spin state might be in the in-plane of the porphyrin ring. NO-ferric Mb gives a typical hemochromogen type

spectrum of the ferrous low spin state, where the iron atom sits in the in-plane of the porphyrin ring. It seems reasonable to assume that the configuration of the heme moiety remains unchanged after departure of NO by photolysis. This contrasts with the out-of-plane structure seen in native ferric Mb. The broad absorption band from 600 to 690 nm, may also come from such a unique configuration.

The EPR measurements also give the direct evidence that the photodissociated product of NO-ferric Mb is in the ferric high spin state, as judged from the absorption at $g = 5.8$ and the coincidence in the angular dependency of the g -tensors in the single crystal for acid-ferric Mb and the photolyzed product. The shift of the principal g value from 6.0 to 5.8 by the conversion to pentacoordination is not yet well analyzed, but it is emphasized that EPR as well as optical absorption can discriminate between the hexacoordinated and pentacoordinated ferric high spin states. The broad EPR signal with the g value of 2.86 (Fig. 6-4) is not yet characterized. It may not originate from the ferric iron atom, since the angular dependency of the g -tensor differed from that of the $g = 5.8$ signal. The $g = 3$ signal is more intensified in the case of NO-ferric HRP. The signal at $g = 3$ in low temperature photolysis has already been reported with cobaltous substituted Mb or Hb [8].

In contrast to the case of NO-ferric Mb, it is striking that the optical absorption spectrum of photodissociated product of

NO-ferric HRP is identical to that of native ferric HRP. This suggests that the iron of native ferric HRP is present in a pentacoordinated structure. The EPR spectrum of the photodissociated product becomes identical to that of ferric HRP [11] after the temperature of the photodissociated sample was once raised to 77 K. It should be noted that only broad EPR absorption spectrum did not change. When NO-ferric HRP was illuminated at 77 K, the co-existence of signal at $g = 6.46$ and 5.38 and a broad signal at $g = 3.08$ was observed. This suggests that the failure to detect the high spin EPR absorption in the $g = 6$ region may come from some peculiar magnetic interaction between the iron atom and an unidentified paramagnetic species, possibly the photodissociated NO molecule. The elevation of the temperature may cause rearrangement of the conformation in the heme crevice, resulting in elimination of such magnetic interaction.

There have been many discussions on the coordination structure of HRP, especially as to the possibility of vacancy at the 6th position. The present findings (cf. Figs. 6-3 and 6-5) are compatible with the pentacoordinated form.

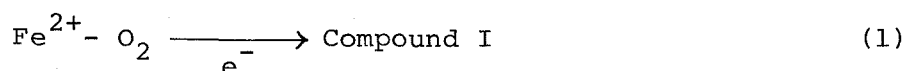
6-5. References

- [1] P. D. Pulsinelli, M. F. Perutz, and R. L. Nagel, *Proc. Natl. Acad. Sci.*, 70, 3870 (1973).
- [2] L. Stryer, J. C. Kendrew, and H. C. Watson, *J. Mol. Biol.*, 8, 96 (1964).
- [3] M. Tamura, K. Kobayashi, and K. Hayashi, *FEBS Lett.*, 88, 124 (1978).
- [4] B. M. Hoffman and Q. H. Gibson, *Proc. Natl. Acad. Sci.*, 75, 21 (1978).
- [5] L. M. Schannon, E. Kay, and J. Y. Lew, *J. Biol. Chem.*, 241, 2166 (1966).
- [6] I. Yamazaki, K. Yokota, and K. Shikama, *J. Biol. Chem.*, 239, 4151 (1964).
- [7] K. Nagai, H. Hori, S. Yoshida, H. Sakamoto, and H. Morimoto, *Biochim. Biophys. Acta*, 532, 17 (1978).
- [8] T. Iizuka, H. Yamamoto, M. Kotani, and T. Yonetani, *Biochim. Biophys. Acta*, 35, 126 (1974).
- [9] T. Yonetani, H. Yamamoto, J. E. Erman, J. S. Leigh, and G. H. Reed, *J. Biol. Chem.*, 247, 2447 (1972).
- [10] S. Yoshida, T. Iizuka, T. Nozawa, and M. Hatano, *Biochim. Biophys. Acta*, 405, 122 (1975).
- [11] M. Tamura and H. Hori, *Biochim. Biophys. Acta*, 284, 20 (1972).

CHAPTER 7. One electron Reduction in Oxyform of Hemoproteins

7-1. Introduction

Five oxidation-reduction states of HRP are known. These states are ferrous, ferric, Compound I, Compound II and Compound III. Of these oxidation reduction states, Compound III of HRP is of great interest in the following points: 1. Though Compound III is known to be an oxyform structure like MbO₂ and HbO₂ [1-3], its physicochemical properties differ from those of MbO₂ and HbO₂. The oxyform of HRP undergoes spontaneous decay to ferric enzyme with a half-time of several minutes [1-5], and it reacts with a number of hydrogen donors [4-6]. These facts suggest that molecular oxygen coordinated to heme iron of HRP is more reactive than those of MbO₂ and HbO₂. 2. Compound III also can be formed by the reaction of Compound II with hydrogen peroxide [7], suggesting that oxy HRP and Compound I are known to retain three and two oxidizing equivalents, respectively, compared with the ferric enzyme, i.e. oxy HRP is at one equivalent oxidized state above Compound I. This was supported by the work of Tamura et al. [4], who proposed that the reduction of oxy HRP to the ferric enzyme consists of three 1-electron steps via Compound I and Compound II as intermediates. A similar mechanism was proposed in the reaction of oxy HRP with ferrous HRP by Phelps et al. [8]. The 1-electron reduction of oxy HRP to Compound I in reaction (1), however, has not yet observed directly.



This difficulty comes from the fact that the reaction products, Compound I and Compound II, further react with reducing agents and oxy HRP [4].

On the other hand, e_{aq}^- is a powerful reducing agent and was found to reduce rapidly the ferric heme of cyt c [9-11], Mb [12, 13], HRP [14] and cytochrome P-450 [15] ($k = 10^{10} - 10^{11} \text{ M}^{-1}\text{s}^{-1}$). With the pulse radiolysis technique it is possible to produce e_{aq}^- within ns time scale to follow the subsequent absorbance change spectrometrically. Therefore, one might expect to observe the unstable intermediates after reduction and the subsequent reaction steps.

In this chapter, the reaction of e_{aq}^- with oxyform of hemoproteins such as MbO_2 and oxy HRP was investigated, where attempts are made to confirm the occurrence of the reaction (1).

7-2. Materials and Methods

HRP and MbO_2 were purified as described in CHAPTER 6 [16, 17]. The enzyme used ($\text{RZ} = 3.2$) was a main fraction absorbed on the CM-cellulose column. Diacetyldeutero HRP was prepared by recombination of apo-HRP with diacetyldeutero heme, followed by DEAE- and CM-cellulose column chromatography by the method of Tamura et al. [18]. All other reagents were obtained commercially as the analytical grade.

A solution of 10^{-3}M phosphate buffer (pH 6-8), or 10^{-2}M borate buffer (pH 8-9) and 0.1 M t-butyl alcohol for scavenging the OH radical were deaerated by extensive flushing with argon.

A concentrated solution of MbO₂ was deoxygenated separately by extensive flushing with nitrogen and added to the deaerated solutions.

Thereafter, the solution was flushed very gently for 30 min with a gas mixture of 2% O₂ and 98% N₂.

A CO complex (Fe²⁺-CO) of diacetyldeutero HRP was prepared by the addition of 2- to 3-fold excess amounts of sodium dithionite to the enzyme in a solution saturated with CO, and the CO-HRP was passed through a Sephadex G-25 column to eliminate excess sodium dithionite in the dark at 0°C. Thereafter, the solution was photolyzed by a 500 W tungsten lamp at room temperature for 2 min, to yield the oxy HRP. This solution of oxy HRP was deaerated by extensive flushing with argon and added to the deaerated solutions containing 10⁻³ M phosphate buffer (pH 6-8) and 0.1 M t-butyl alcohol.

The bottle containing approximately 200 ml of sample solution was connected to the flow cell with 1 or 1.5 cm light path, placed in the front of the accelerator. It was necessary to replace the solution in the irradiation cell with fresh solution after each irradiation. The pulse radiolysis experiments were performed with the electron linear accelerator of the Institute of Scientific and Industrial Research, Osaka University. The pulse-width and energy were 10 ns and 20 MeV, respectively. Dosimetry was performed by measurement of e_{aq}⁻ absorption. The light source was a 1 KW xenon lamp. A Nikon monochromator was used in conjunction with appropriate light filter to eliminate second order components in the light. Slit width was adjusted between 1-2.5 mm. A 1 P-28 photomultiplier was used. Photolysis

by the analyzing light was minimized by means of an optical shutter and selected filters.

Optical absorption spectra were measured with Cary-118 spectrometer. The absorption spectrum of Compound I of diacetyldeuteroHRP was measured in the stopped flow apparatus to obtain kinetic difference spectrum. For this measurement, the ferric diacetyldeutero HRP was mixed with 2-,3-fold excess amounts of hydrogen peroxide to the enzyme. The stopped flow method was measured with a Union Giken spectrometer model RA-401.

7-3. Results

7-3-1. MbO₂

After an electron pulse, rapid absorption changes were observed over the whole wavelength range from 370 to 700 nm. Fig. 7-1-(1) shows the rapid increase in absorption at 600 nm due to the generation of e_{aq}^- and the subsequent decrease caused by the decay of e_{aq}^- . The decay of e_{aq}^- accompanied the absorption increase at 430 nm and the absorption decrease at 410 nm, as shown in Figs. 7-1-(2) and (3).

Fig. 7-2-(1) shows the first order plots of decay of e_{aq}^- at 600 nm and the reaction of MbO₂ at 410 nm. First order reaction kinetics are observed which is to be expected since the concentration ratio $[MbO_2]/[e_{aq}^-] > 10$. It is noted that the rate of the disappearance of e_{aq}^- is larger than that of the reaction of MbO₂, suggesting that a part of e_{aq}^- reacts with O₂. The apparent rate constants are plotted against MbO₂ concentration in Fig. 7-2-(2), giving the straight line.

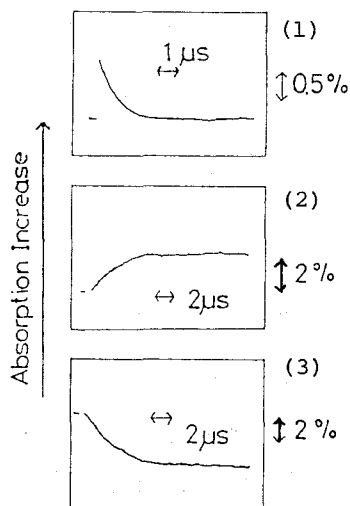


Fig. 7-1. The oscilloscope traces of the transmittance change after pulse radiolysis of MbO_2 measured (1), at 600 nm (2), at 410 nm (3), at 430 nm. Phosphate buffer (pH 7.4), 10^{-3} M

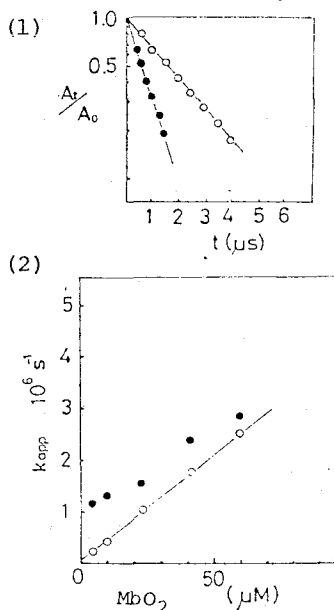


Fig. 7-2: (1) First order plots calculated from the traces shown in Fig. 7-1; ●, decay of e_{aq}^- measured at 600 nm, ○, growth of Soret absorption at 450 nm. (2) Concentration dependence of the pseudo-first order rate constants for reaction e_{aq}^- with MbO_2 . ●, decay of e_{aq}^- measured at 600 nm; ○, growth of Soret absorption at 450 nm.

The pseudo-first order of the disappearance of e_{aq}^- increased with increment of the concentration of MbO_2 . This suggests that the absorption change of Fig. 7-1 is followed by the reaction MbO_2 with e_{aq}^- . This is analyzed as follows. The rate of the disappearance of e_{aq}^- is expressed by Eq. (2),

$$-\frac{d[e_{aq}^-]}{dt} = \{k_1[O_2] + k_2[MbO_2]\}[e_{aq}^-] \quad (2)$$

where k_1 and k_2 are the rate constants of the reaction of e_{aq}^- with O_2 and MbO_2 , respectively. From Eq.(2), the apparent rate constants (k_{app}) determined at 600 nm and 410 nm can be expressed by Eq. (3) and (4) respectively.

$$k_{app \ 600 \text{ nm}} = k_1[O_2] + k_2[MbO_2] \quad (3)$$

$$k_{app \ 410 \text{ nm}} = k_2[MbO_2] \quad (4)$$

Therefore the difference between $k_{app \ 410 \text{ nm}}$ and $k_{app \ 600 \text{ nm}}$ depends on the concentration of O_2 . From the slope of Fig. 7-2-(2), k_2 is estimated. The second order rate constant for the reaction e_{aq}^- with MbO_2 at pH 7.4 is $4 \times 10^{10} \text{ M}^{-1}\text{s}^{-1}$, which is near the diffusion controlled rate.

The difference spectrum at 8 μs after the pulse, at which time no measurable e_{aq}^- remains, is shown in Fig. 7-3-(1). The spectrum has an absorption maximum at 410 nm and an absorption minimum at 430 nm in the Soret region together with distinct absorption minima at 545 nm and 575 nm. It also has broad peaks around 500 nm and from 600 to 700 nm. The shape of the difference spectra were not affected by pH from 6.5 to 8.4.

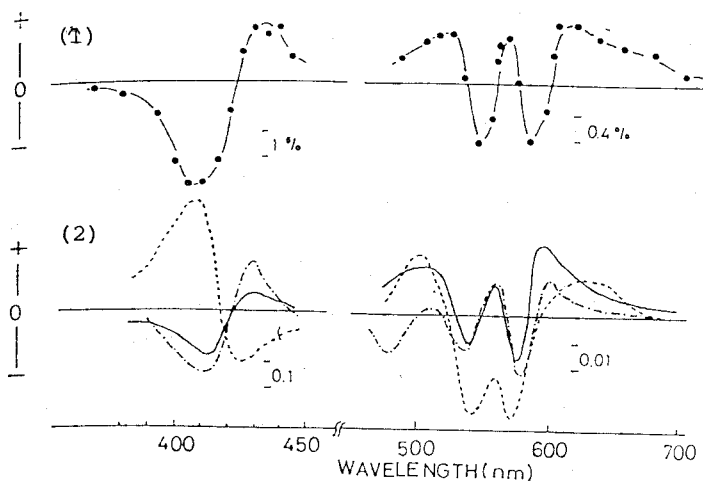


Fig. 7-3. (1) Kinetic difference spectrum of pulse radiolysis of MbO_2 . The spectrum is taken at $8 \mu\text{s}$ after pulse radiolysis. Phosphate buffer (pH 7.4), 10^{-3} M. (2) Difference spectra of MbO_2 minus ferric Mb (\cdots), ferrous Mb ($-\cdot-\cdot-$), and hydrogen peroxide-induced compound (---), respectively.

Fig. 7-3-(2) shows the difference spectra of MbO_2 minus ferric Mb (\cdots), ferrous Mb ($-\cdot-\cdot-$), and hydrogen peroxide-induced compound, the so-called "ferryl" Mb (---), respectively at pH 7.4. It is noted that the kinetic difference spectrum in Fig. 7-3-(1) is similar to the difference spectrum of MbO_2 minus hydrogen peroxide-induced compound, not ferric Mb or ferrous Mb. Therefore it is concluded that absorption change in Fig. 7-1 is due to the reaction of e_{aq}^- with MbO_2 , followed by the formation of ferryl Mb.

7-3-2. Oxy HRP

The native oxy HRP autodecomposes into the ferric enzyme so

rapidly (half-life at 20°C; 4 min) that the reaction oxy HRP with e_{aq}^- could not be performed by the present method. In contrast to native HRP, the oxyform of artificial HRP, containing 2,4 diacetyldeuterohematin in the place of protohematin IX of natural HRP, is very stable and can be kept at room temperature for a few hours without changes in the absorption spectrum [5]. Therefore, oxy diacetyldeutero HRP was used in the present experiments.

The optical absorption spectra of diacetyldeutero HRP and their derivatives are shown in Fig. 7-4. Upon addition of hydrogen peroxide to the ferric diacetyldeutero HRP, Compound II was formed spontaneously via Compound I and the compound thus formed was quite stable. Because of the instability of Compound I of diacetyldeutero HRP, its spectrum was obtained by the use of the stopped flow technique between the ferric diacetyldeutero HRP and hydrogen peroxide.

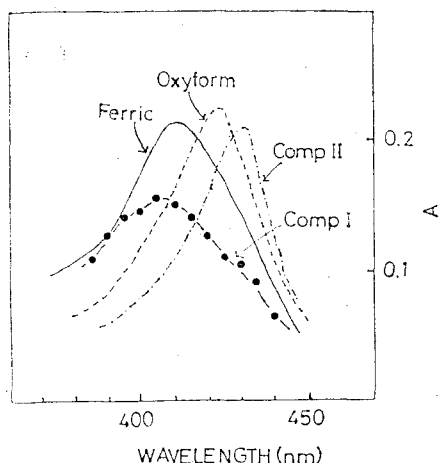


Fig. 7-4. Comparison of optical absorption spectra of ferric diacetyldeutero HRP and its hydrogen peroxide-induced compounds. Phosphate buffer (pH 7.4), 0.1 M. Compound II was formed by the addition of 7 μ M hydrogen peroxide. The absolute spectrum of Compound I was calculated from the kinetic difference spectrum of the reaction ferric enzyme with hydrogen peroxide.

Fig. 7-5 shows the time course of the absorption change at different wavelengths after an electron pulse of oxy diacetyldeutero HRP. The absorption at 420 nm near the absorption maximum of oxy HRP decreased (Fig. 7-5-(2)) with the decrease of e_{aq}^- at 600 nm (Fig. 7-5-(1)). A similar time course of absorption change was also seen at 370 nm in Fig. 7-5-(3).

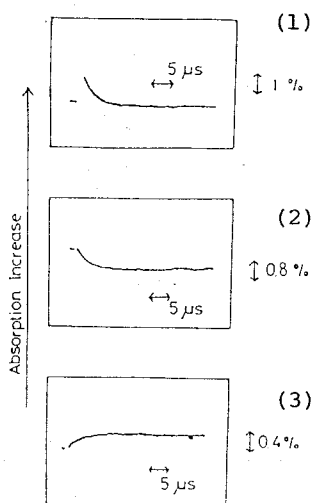


Fig. 7-5. The oscilloscope traces of the transmittance change after pulse radiolysis of oxy diacetyldeutero HRP measured at (1) 600 nm, (2) 420 nm, and (3) 370 nm. Phosphate buffer (pH 7.4), 10^{-3} M.

Fig. 7-6 shows the first order plots of the decay of e_{aq}^- at 600 nm and the reaction of oxy HRP at 420 nm. The rate of the disappearance of e_{aq}^- is found to be almost identical to that of the reaction of oxy HRP. The second order rate constant for the reaction e_{aq}^- with oxy HRP at pH 7.4 is $4 \times 10^{10} \text{ M}^{-1} \text{ s}^{-1}$. As ferrous HRP is not formed in the deaerated solution [19], the concentration of dissolved oxygen molecule was less than 10^{-6} M. Therefore, the reaction O_2^- with oxy HRP can be ruled out.

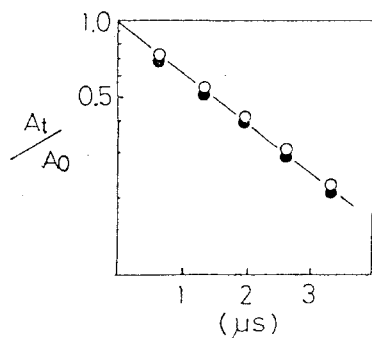


Fig. 7-6. First order plots calculated from the traces of Fig. 7-5; ●, data obtained at 600 nm, and ○, at 420 nm.

The difference spectrum obtained at 10 μ after an electron pulse is shown in Fig. 7-7-(1). The spectrum, which has an absorption minimum around 390 nm, is similar to the difference spectrum of oxy diacetyldeutero HRP minus Compound I of this enzyme only. Therefore, it is concluded that oxy HRP reacts with e_{aq}^- to form Compound I.

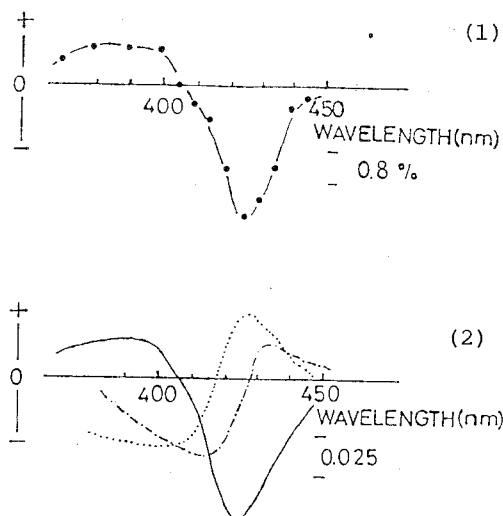
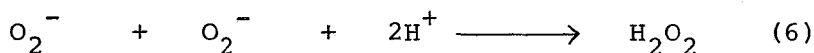
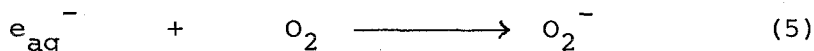


Fig. 7-7. (1) Kinetic difference spectrum of pulse radiolysis of oxy diacetyldeutero HRP. The spectrum is taken at 8 μ s after pulse radiolysis. Phosphate buffer (pH 7.4), 0.1 M. (2) Difference spectra of oxy diacetyldeutero HRP (···), Compound I (—), and Compound II (-·-·). Phosphate buffer (pH 7.4), 0.1 M.

7-4. Discussion

In the presence of oxygen, e_{aq}^- reduces O_2 to form O_2^- with the rate constant of $2 \times 10^{10} \text{ M}^{-1}\text{s}^{-1}$ [20], and H_2O_2 can be generated by the disproportionation of O_2^- with the rate constant of $3 \times 10^5 \text{ M}^{-1}\text{s}^{-1}$ at pH 7.4 [21], as shown by reactions (5) and (6).



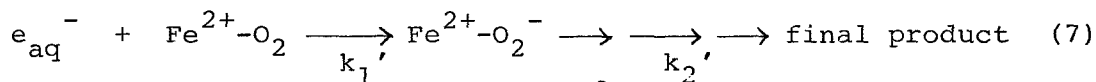
Therefore, in the case of MbO_2 , the alternative reaction of MbO_2 with O_2^- or H_2O_2 may be taken into account. This possibility, however, can be excluded by the following reasons.

- (1) The pseudo first order rate of the disappearance of e_{aq}^- increased with the increment of the concentration of MbO_2 as shown in Fig. 7-2, suggesting that a considerable part of e_{aq}^- reacts with MbO_2 .
- (2) Under the oxygen-saturated condition, any reactions MbO_2 with O_2^- or H_2O_2 were not observed in the μs time scale.

Futhermore, the reactivity of O_2^- or H_2O_2 with MbO_2 was examined. It was found that O_2^- , which is produced by the xanthine oxidase-catalyzed oxidation of xanthine, is very unreactive with MbO_2 and disappears as a result of interaction with each other (reaction (6)), as observed in the reaction HbO_2 with O_2^- [22]. In static experiments, H_2O_2 was found to react slowly with MbO_2 to generate the optical spectrum of ferryl Mb, as observed in the reaction leghemoglobin with H_2O_2 [23]. This reaction, however, took more than 1 min, to reach completion. Therefore, it can be said that

under the conditions employed here O_2^- does not contribute to the reduction of MbO_2 .

In the reaction e_{aq}^- with both MbO_2 and oxy HRP, e_{aq}^- reduces apparently the redox site of oxyheme in a direct reaction. These reactions, however, can be interpreted by the following sequence events as reaction (7):



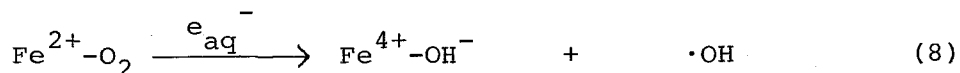
An initial step is the formation of $Fe^{2+}-O_2^-$. Then the intermolecular electron transfer from heme iron to the ligand forming $Fe^{3+}-O_2^{2-}$ or $Fe^{4+}-O_2^{3-}$, and rapid association of H^+ and a loss of water molecule would lead to the observed final product. At low concentration of oxyhemoproteins, k_1' is rate-determining, while at the higher concentration it may be anticipated that k_2' becomes rate-determining ($k_2' < k_1'[Fe^{2+}-O_2]$). To examine this possibility, at high concentration of MbO_2 ($> 100 \mu M$) the reaction time course of MbO_2 was measured in the range between 500 and 700 nm. In this case, however, there was no obvious spectral indications of intermediates at any wavelength. This suggests that the process from $Fe^{2+}-O_2^-$ to the final product occurs long before 70 ns, i.e. the rate constant of k_2' would be greater than $10^7 s^{-1}$.

Yamazaki et al. [24] have proposed a general scheme of five oxidation-reduction states, which exist in the oxidative function of HRP. In this scheme, the reaction from oxy HRP to Compound I (reaction (1)) could be observed directly by the use of the pulse radiolysis technique. This reaction is considered to correspond to change of "effective oxidation states" from +6 to +5. The general

scheme in HRP proposed by Yamazaki et al. [24] is expanded here to oxidation-reduction states of Mb. MbO_2 is considered to be at the oxidation state +6. As ferryl Mb has been believed to be at the oxidation state +4, it seems as if the reaction of Fig. 7-1 was 2-electron reduction of MbO_2 (+6) to ferryl Mb (+4) via the +5 state. This possibility, however, can be ruled out by the following reasons. The ratio 0.01 for $[\text{e}_{\text{aq}}^-]/[\text{MbO}_2]$ is too small to permit a significant amount of 2-electron reduction to take place. Furthermore, the second order kinetics, as shown in Fig. 7-2, are not compatible with 2-electron reduction. In addition, the shape of difference spectra in Fig. 7-3-(1) were not affected by the ratio $[\text{e}_{\text{aq}}^-]/[\text{MbO}_2]$. Therefore this reaction is considered to be 1-electron reduction. The oxidation state +5, which corresponds to Compound I of HRP, was not detected. In this case the fate of one more equivalent is not known. At present, two possible reaction mechanisms for the formation of ferryl Mb are considered as follows.

- (1) The first initial formation of a +5 oxidation state is the rate determining step, which then undergoes extremely rapid reduction to ferryl Mb by a reducing group, e.g. an amino acid residue [25, 26]. Any such intermediates, however, could not be detected in the present experiments. Therefore if +5 oxidation state of Mb, which is similar to Compound I of HRP, exists, the life time of this compound is shorter than 70 ns.
- (2) The electron transfer from the heme iron to molecular oxygen

gives rise to $\cdot\text{OH}$ as the reduction product of bound dioxygen, as Eq. (8).



In the oxidation of ferric Mb by H_2O_2 , the production of $\cdot\text{OH}$, which is similar to the ferrous ion reaction, the so-called Fenton-like reaction, was suggested by George et al. [27].

If the latter mechanism occurs, the +5 oxidation state of Mb does not exist.

The reaction of oxyheme with e_{aq}^- is analogous to that proposed for the oxidation of substrate by cytochrome P-450 [28, 29], and for hydroxylation of α methene bridge of heme in the heme oxygenase reaction [30, 31]. The identity of 1-electron reduction state in the oxygenated cytochrome P-450 has been received much attention. Recently, organic hydroperoxide could replace NADPH and molecular oxygen in supporting the hydroxylation of various substrates [32-35]. From these studies, it was proposed that the higher oxidation state of cytochrome P-450, which corresponds to Compound I or Compound II of HRP, is the common "active oxygen" species in these hydroxylations. This proposal, however, has not been proven directly. The present observation suggests that the 1-electron reduction state of the oxygenated cytochrome P-450 may be also the ferryl state of this enzyme.

7-5. References

- [1] I. Yamazaki and K. Yokota, *Biochim. Biophys. Res. Commun.*, 19, 249 (1965).
- [2] A. Wittenberg, R. W. Noble, A. Wittenberg, A. Antonini, M. Brunori, and J. Wyman, *J. Biol. Chem.*, 242, 626 (1967).
- [3] I. Yamazaki, K. Yokota, and M. Tamura, "in Hemes and Hemoproteins" B. Chance, E. Estabrook, and T. Yonetani eds. p. 319, Academic Press, New York, 1966.
- [4] M. Tamura and I. Yamazaki, *J. Biochem.*, 71, 311 (1972).
- [5] R. Makino, H. Yamada, I. Yamazaki, *Arch. Biochem. Biophys.*, 173, 66 (1976).
- [6] K. Yokota and I. Yamazaki, *Biochem. Biophys. Res. Commun.*, 18, 48 (1965).
- [7] J. George, *J. Biol. Chem.*, 201, 427 (1953).
- [8] C. F. Phelps, E. Antonini, G. Giacometti, and M. Brunori, *Biochem. J.*, 141, 265 (1974).
- [9] E. J. Land and A. J. Swallow, *Arch. Biochem. Biophys.*, 45, 365 (1971).
- [10] I. Pecht and M. Faraggi, *Proc. Natl. Acad. Sci. U. S. A.*, 69, 902 (1972).
- [11] J. Wilting, K. J. H. Van Buuren, R. Braams, and B. F. Van Gelder, *Biochim. Biophys. Acta.*, 376, 285 (1975).
- [12] J. Wilting, A. Raap, R. Braams, S. H. De Bruin, H. S. Rollema, and L. H. Janssen, *J. Biol. Chem.*, 249, 6325 (1974).
- [13] J. R. Clement, N. T. Lee, H. Klapper, and L. M. Dorfman, *J. Biol. Chem.*, 251, 2077 (1976).

- [14] K. Hayashi, D. Lindenau, and M. Tamura, *Adv. Exp. Med. Biol.*, 94, 353 (1977).
- [15] P. Debey, E. J. Land, R. Santus, and A. J. Swallow, *Biochem. Biophys. Res. Commun.*, 86, 953 (1979).
- [16] I. Yamazaki, K. Yokota, and K. Shikama, *J. Biol. Chem.*, 239, 4151 (1964).
- [17] L. M. Schannon, E. Kay, and J. Y. Lew, *J. Biol. Chem.*, 241, 2166 (1966).
- [18] M. Tamura, T. Asakura, and T. Yonetani, *Biochim. Biophys. Acta*, 268, 292 (1972).
- [19] R. Makino and I. Yamazaki, *J. Biochem.*, 72, 655 (1972).
- [20] M. Anbar, M. Bamberg, and A. B. Ross, *Selected Specific Rates of Reactions of Transients from Water in Aqueous Solutions. 1. Hydrated Electron*, United States National Stand and Reference Data System-NBS, 46 (1973).
- [21] D. Behar, G. Cyapski, J. Rabani, L. M. Dorfman, and W. A. Schwary, *J. Phys. Chem.*, 74, 3209 (1970).
- [22] H. C. Sutton, P. B. Roberts, and C. C. Witerbourn, *Biochem. J.*, 155, 503 (1976).
- [23] I. Aviram, B. G. Wittenberg, and J. B. Wittenberg, *J. Biol. Chem.*, 253, 5685 (1978).
- [24] H. Yamada and I. Yamazaki, *Arch. Biochem. Biophys.*, 165, 728, (1974).
- [25] T. Shiga and I. Imaizumi, *Arch. Biochem. Biophys.*, 167, 469, (1975).
- [26] J. F. Gibson, D. J. E. Ingram, and P. Nicholls, *Nature*, 181, 1398 (1958).

- [27] P. George and D. H. Irvine, *J. Colli, Sci.*, 11, 327 (1956).
- [28] C. A. Tyson, J. D. Lipscomb, and I. C. Gunsalus, *J. Biol. Chem.*, 247, 5777 (1972).
- [29] Y. Ishimura, V. Ullrich and J. A. Peterson, *Biochem. Biophys. Res. Commun.*, 42, 140 (1971).
- [30] T. Yoshida and G. Kikuchi, *J. Biol. Chem.*, 253, 4230 (1978).
- [31] T. Yoshida, M. Noguchi, and G. Kikuchi, *J. Biol. Chem.*, 255, 4418 (1980).
- [32] A. D. Tahimtula, P. J. O' Brien, E. G. Herycay, J. A. Peterson, and R. W. Estabrook, *Biochem. Biophys. Res. Commun.*, 60, 695 (1974).
- [33] E. G. Hrycay, J-A, Gustafsson, *Biochem. Biophys. Res. Commun.*, 66, 209 (1975).
- [34] F. Lichtenberger, W. Nastainczyk, and V. Ullrich, *Biochem. Biophys. Res. Commun.*, 66, 209 (1975).
- [35] R. C. Blake and M. J. Coon, *J. Biol. Chem.*, 255, 4100 (1980).

CONCLUSION

The purpose of this study is to clarify structure origin of great differences in biological function between Mb and HRP by several physico-chemical methods.

Ferrous hemoproteins

CHAPTERS 1, 2 and 3 deal with the electronic structure of the ferrous hemoproteins and their model systems. Because of the diamagnetic nature of the ferrous state, NO radical was used as a probe for elucidating the structure of the heme environment of hemoproteins. In these studies, the second derivative technique was employed for detecting the small changes of the spectra, which are hardly quantitized in the normal first derivative display.

In CHAPTER 1, in order to interpret the EPR spectra for the NO complex of the ferrous hemoproteins, the EPR spectra of NO-ferrous heme-nitrogen base (pyridine and imidazole derivatives) were measured. From the analysis of EPR parameters, the change in EPR pattern of NO-ferrous HRP can be attributed to the NO ligand with surrounding amino acid residues, not to the nature of the iron-proximal histidine. It appears that the Fe-N-O unit is more bent than those of Mb and model compounds.

In CHAPTER 2, the pH-dependence of the EPR spectra of NO-ferrous Mb was examined, and the heme-linked ionization group having $pK = 7$ was detected with NO-ferrous Mb. The possible participation of the distal histidine was discussed for this ionization group.

In CHAPTER 3, the technique of the EPR measurement on the NO complex was applied to the synthetic polymer systems. It was demonstrated that the linkage between NO and ferrous heme iron was altered by the expansion of polymer chain.

Ferric hemoproteins

CHAPTERS 4, 5 and 6 deal with the kinetic analysis and the structure of ferric hemoproteins.

It has been believed that only ferrous complexes are photo-dissociable. In CHAPTER 4, however, photodissociation phenomenon has firstly been observed with the ferric NO complex.

The ability of the photodissociation of NO complexes into the ferric state was applied to the kinetic studies of ligand binding in CHAPTER 5. The kinetic difference spectra of NO-ferric Mb showed that the native ferric Mb (aquao form) appeared within 1 ms after photodissociation on NO by photolysis. This was confirmed by the kinetic analysis of the recombination of NO with ferric Mb. In contrast to NO-ferric Mb, NO-ferric HRP gave different kinetics of NO binding for the flash photolysis and the stopped flow methods at alkaline pH. The kinetic difference spectra showed that the acid form, but not the alkaline form, appeared first upon photolysis of NO-ferric HRP even at alkaline pH. The data obtained here were compatible with the assumption that the formation of the alkaline form of the enzyme is the coordination of OH^- at the 6th position, which is vacant at acidic pHs.

In CHAPTER 6, in order to generate and trap the penta-coordinated ferric heme, the photolysis of NO-ferric hemoproteins

was performed at liquid helium temperature (4.2 K). As the recombination process cannot occur at such low temperature, optical and EPR spectra of the pentacoordinated form can be measured. The optical and EPR spectra of the photolyzed product of NO-ferric Mb were different from those of native ferric Mb in both acid and alkaline forms. Taking account of the fact that the water molecule coordinates at the 6th position in the native ferric Mb, it was concluded that the photodissociated product of NO-ferric Mb at 4.2 K is present in the pentacoordinated form. In contrast to the results of NO-ferric Mb, any significant difference in optical and EPR spectra between the photodissociated product of NO-ferric HRP and the native ferric HRP could not be detected. This indicates that the 6th position of the heme iron of native ferric HRP is vacant.

Higher oxidation states of hemoproteins

CHAPTER 7 deals with the higher oxidation states of hemoproteins by the use of pulse radiolysis technique. Attention was focussed on the presence or absence of Compound I in Mb. The reaction of e_{aq}^- , which is generated by the pulse radiolysis in aqueous solution, with oxyform of hemoproteins was performed. In these studies, the 1-electron reduction of oxy HRP to Compound I was observed directly. In contrast to oxy HRP, MbO_2 was reduced by e_{aq}^- to form the hydrogen peroxide-induced compound (ferryl Mb), and the oxidation state, which corresponds to Compound I of HRP, was not detected. From these results, it was considered that the oxidation state of Compound I in Mb does not exist.

LIST OF PUBLICATION

The content of this thesis is composed of the following papers;

- [1] Electron Paramagnetic Resonance of NO-Heme-Nitrogen Base
Kazuo Kobayashi, Mamoru Tamura, and Koichiro Hayashi,
Biochim. Biophys. Acta, 70, 23 (1982).
- [2] The NO-Probed Detection of the Heme-Linked Ionization Group
of Myoglobin
Mamoru Tamura, Kazuo Kobayashi, and Koichiro Hayashi,
Biochem. Biophys. Res. Commun., 70, 265 (1976).
- [3] Electron Paramagnetic Resonance of Nitric Oxide-Heme-Polymer
Complex
Kazuo Kobayashi, Mamoru Tamura, and Koichiro Hayashi,
Chem. Lett., 1181 (1976).
- [4] Flash Photolysis Studies on Nitric Oxide Ferrihemoprotein
Complexes
Mamoru Tamura, Kazuo Kobayashi, and Koichiro Hayashi,
FEBS Lett., 88, 124 (1978).
- [5] Kinetic Analysis of the Recombination of NO with Ferri-
hemoproteins
Kazuo Kobayashi, Mamoru Tamura, and Koichiro Hayashi,
Biochemistry, 21, 729 (1982).
- [6] Photodissociation Phenomena of NO-Ferrihemoprotein Complexes
Mamoru Tamura, Kazuo Kobayashi, Koichiro Hayashi, and
Hiroshi Hori,

"Oxidase and Related Redox Systems" H.S. Mason, T.E. King, and M. Morrison, Eds., Vol. III, Academic Press, New York, 685 (1982).

- [7] Electron Paramagnetic Resonance and Optical Absorption Spectra of the Pentacoordinated Ferrihemoproteins
Kazuo Kobayashi, Mamoru Tamura, Koichiro Hayashi, Hiroshi Hori, and Hideki Morimoto,
J. Biol. Chem., 255, 2239 (1980).
- [8] One Electron Reduction in Oxyform of Hemoproteins
Kazuo Kobayashi and Koichiro Hayashi,
J. Biol. Chem., 256, 12350 (1981).

The other supplementary papers:

- [1] Immobilization of Hemoglobin by Radiation-Induced Polymerization
Miyako Miki, Kazuo Kobayashi, Koichiro Hayashi, and Mamoru Tamura,
Biotechnol. Bioeng., 24, 2587 (1982).
- [2] One Electron Reduction of D Amino Acid Oxidase
Kazuo Kobayashi, Koichi Hirota, Hitomi Ohara, Koichiro Hayashi, Retsu Miura, and Toshio Yamano,
Biochemistry, 22, 2239 (1983).
- [3] Application of Pulse Radiolysis to Biochemistry
Kazuo Kobayashi and Koichiro Hayashi,
"Fast Methods in Physical Biochemistry and Cell Biology"
R. Sha'afi and R. Fernandez, Eds., Elsevier North-Holland Biomedical Press, p. 87 (1983).

[4] The Reaction of Superoxide Radical with Catalase:
Mechanism of the Inhibition of Catalase by Superoxide
Radical

Norihide Shimizu, Kazuo Kobayashi, and Koichiro Hayashi,
J. Biol. Chem., in press.

ACKNOWLEDGEMENT

The work of this thesis was performed under the guidance of Professor Koichiro Hayashi, the Institute of Scientific and Industrial Research, Osaka University.

The author wishes to express his deep gratitude to Professor Koichiro Hayashi for his continuous guidance and encouragement.

The author is greatly indebted to Dr. Mamoru Tamura, the Institute of Applied Electricity, Hokkaido University, for his intimate guidance and stimulating discussions.

The author wishes to thank Dr. Masahiro Irie, Dr. Yukio Yamamoto, and Mrs. Miyako Miki for their valuable discussions and helpful suggestions.

Much thanks is given to Dr. Hideki Morimoto and Dr. Hiroshi Hori of the Faculty of Engineering Science, Osaka University, for their helpful discussions and the use of EPR and optical absorption spectroscopy at liquid helium temperature.

The author is grateful to Dr. A. John Swallow in Paterson Laboratories, U.K., for his guidance of the pulse radiolysis.

The author thanks Mr. Kunihiko Tsumori, Mr. Norio Kimura, Mr. Tamotsu Yamamoto, Mr. Toshihiko Hori in the Radiation Laboratory, the Institute of Scientific and Industrial Research, Osaka University for their assistance in operating the accelerator.

Thanks are also due to all the members of Hayashi Laboratory for their kind assistance.

Finally, the author would like to thank his father Tsutomu

Kobayashi and his mother Mitsue Kobayashi for their encouragement and assistance.

March, 1984

K. Kobayashi

Kazuo Kobayashi